Master Thesis

Mechanical properties of cells probed by atomic force microscopy

Dmitry Morozov

Supervisors:

Univ.Prof. Dr. José Luis Toca-Herrera

Institute for Biophysics, Department of Nanobiotechnology

University of Natural Resources and Life Sciences, Vienna

DI Andreas Weber, BSc

Vienna, 2020

Table of content

Abstract

Atomic force microscopy (AFM) is widely used to study various biological objects, among others also mammalian cells in physiologically adequate conditions. Force-distance curves provide information about mechanical characteristics of the cell, such as contact stiffness, deformation, Young's modulus etc. Such properties have been linked to various states of disease. AFM studies of the morphology and mechanical properties of native cells can be used in biomedical applications, such as determining the physiological and pathological states of cells. In this work, AFM was applied to examine the mechanical properties of the human umbilical vein endothelial cells (HUVEC) and their dependence on different measurement settings. The influence of the loading rate, maximum load and indenter geometry on the measurement of mechanical properties of such cells has been studied. By applying a linear fitting to a Force-Distance-Curves obtained during nanoindentation experiments the stiffness and the Young's modulus were calculated. Relation of the mechanical properties of the cells and the experiment condition was demonstrated. Obtained results can be used in a further studies to compare viscoelastic properties of the approach and the retracting curve.

Abbreviations

AFM	Atomic Force Microscopy
δ	Indentation [m]
DMEM	Dulbecco Modified Eagle Medium
DMSO	Dimethyl sulfoxide
DMT	Derjaguin-Muller-Toporov model
E	Young's Modulus, Elastic Modulus [Pa]
ε	Strain [dimensionless]
EtOH	70% ethanol
F	Force [N]
FCS/FBS	Fetal Calf Serum/Fetal Bovine Serum
HUVEC	Human Umbilical Vein Endothelial Cells
JKR	Johnson-Kendall-Roberts model
k	Stiffness in [N/m]
k_b	Constant of Boltzmann [J/K]
PBS	Phosphate Buffer Saline
rpm	Rounds per minute
σ	Stress [Pa]
T	Temperature [K]
ν	Poisson ratio [dimensionless]
UV/O	UV-Ozone cleaning
Z_p	z-Position of piezoelement [m]

1. Motivation

Over the last dozens of years, the study of cell mechanical properties has become more and more important. The reasons for this are manifold, since cells exist in biological systems where application of external force is ubiquitous. Cells can feel and react to such forces and it has been known for some years that cell function can be controlled by such mechanical stimuli. Many studies have shown that states of disease such as cancer lead to changes in the mechanical properties Thus there is reason to believe that methods to study cell mechanics can be applied for diagnostic purposes. Atomic Force Microscopy is one of the most used applied techniques to study cell mechanics. The measured properties depend on the used measurement settings. Therefore, the main motivation for this study is to understand

- the role of loading rate on cell mechanical properties,
- the role of indenter geometry on cell mechanics,
- the role of different maximum loads.

2. Introduction

A cell is an elementary, smallest living unit of a living organism. Any process in an organism, is determined by the processes occurring in individual cells. The most highly developed and structurally complex systems are eukaryotic cells, which make up all the most advanced multicellular organisms – e.g. plants, animals, humans. Of interest are animal eukaryotic cells. The study of the physiology and pathologies of animal cells allows us to solve the problems of modern medicine: to identify mechanisms of the origin and course of diseases at the cellular level, to find new ways to treat pathological conditions or to synthesize new medical substances. In this case, various types of eukaryotic animal cells are the most important objects of biomedical research in diseases such as cancer, metabolic diseases and many more. Recently, significant successes have been achieved in the study of cells, but there are still plenty of unresolved issues and tasks.

2.1. Cells as biological materials

Cells are complex, hierarchical materials that consist of many different types of molecules whose constant turnover is regulated through complex signaling. Regarding cell shape and mechanics, the most prominent elements of the cell are those of the cytoskeleton (actin, microtubules and the different kinds of intermediary filaments) as well as adhesion molecules [1–4]. It is known that different diseases change the nature of expression of the above-mentioned elements, leading to phenotypes of cells with changes in cell mechanics. In addition, diseases often lead to changes in the build-up of the extracellular matrix (ECM) that surrounds cells in tissue[5–8].

The cells of the body are constantly under external mechanical stress such as e.g. the pressure from other cells, blood pressure, the movement of cells with respect to each other and more. The cells, interact with each other and other surrounding objects, can move in space, change their size and shape. Blood cells are forced to undergo strong deformations, passing through micro-sized capillaries; lung cells stretch when inhaled; myofibrils contract when the striated muscles are strained; the epithelium is deformed when pressed on the skin; vascular endothelium contracts or relaxes in response to changes in blood pressure; fibroblasts move to the site of injury for wound healing. Not surprisingly, the mechanical properties of cells of various types differ significantly and are determined by the specialization and functions of

the cell. due to the expression of genes encoding a set of proteins characteristic of a given cell type[9–13]. A change in the normal mechanical properties of cells can lead to severe negative consequences for the whole organism, the development of pathologies.

The results of studies of the mechanical properties of eukaryotic cells can help in understanding physiological and pathological intracellular molecular processes, facilitate the creation and testing of drugs, determine the effectiveness of the therapy used, shed light on the effect of physical influences and chemicals on cells, including unfavorable environmental factors and toxins. Among the methods for studying the mechanical characteristics of cells, atomic force microscopy (AFM) stands out - it allows to study various properties of a cell with a submicron resolution under conditions as close as possible to physiological ones.

During the MSc thesis, various methods applied to study cellular mechanics will be discussed. Then, as the work of this thesis was performed using AFM, a concise description of principles of AFM will be described. We will then study the influence of loading rate, maximum load and indenter geometry on cell mechanical parameters.

2.2. Mechanical models for living cells

It has been established that the abnormal mechanical properties of individual cells may indicate the course of pathological processes in the body. Due to their complex build-up, cells show viscoelastic properties. It is therefore not easy to determine cell mechanical properties that are feasible to be compared to studies made by other groups in a quantitative way.

2.2.1. Elastic models

Even though cells show viscoelastic properties, a high amount of studies published use Hertzian elastic theory to describe their properties[10,14–20]. In the easiest case, the so-called Young´s Modulus of the sample is determined (from e.g. stress-strain-curves). We first define the stress σ and the strain ε by

$$\sigma = \frac{F}{A} \qquad \textit{Eq. 1}$$

$$\varepsilon = \frac{l - l_0}{l_0} \qquad \textit{Eq. 2}$$

With F being the applied force, A the area of the cross section, l_0 the initial length of the body and l the final length. The Young's Modulus (E, in Pa) is the relation of the stress applied on the cell to the resulting strain

$$E = \frac{\sigma(\varepsilon)}{\varepsilon}. \qquad \textit{Eq. 1}$$

It is a three-dimensional elastic material constant. The equation above is only applicable to materials that are linearly elastic and isotropic. In a stress-strain diagram (as shown in Figure 2-1), the slope of the linear region can be used to determine the Young's modulus.

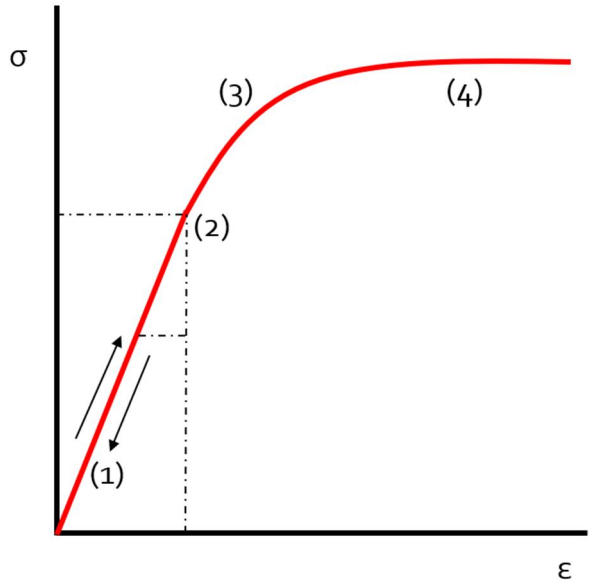

Figure 2-1. Theoretical stress-strain diagram for a material. (1) Elastic deformation happens. (2) Elastic limit is reached. (3) Plastic deformation of the sample and (4) Fracture limit of material.

If we rewrite the relations that are shown above, it leads to a derivation of Hooke's law following

$$F = \frac{EA}{l_0}\Delta l = -kx \qquad \textit{Eq. 2}$$

Where k is the stiffness of the sample and x is a one-dimensional length change. Thus, on the assumptions of the Hertzian mechanical model, it should be possible to derive the Young's Modulus from stress-strain-relations. In brief, the model describes the contact of two ideally elastic bodies. Other assumptions that must be made are (thinking about AFM measurements):

- The sample is assumed as ideal linear elastic isotropic material,

- No other interactions (adhesion, plastic deformation, friction forces) take place,
- Indentation small with respect to measured body size
- Indenter needs to be non-deformable,
- Cross-sectional contact area remains constant.

Clearly, most of those assumptions are violated when measuring cells. Nevertheless, the main body of literature concerned with cell mechanics uses this approach due to the quite easy theory, fast fitting and easy curve preparation.

Currently, the most common models used to determine Young's modulus in AFM are the Hertzian model, Sneddon, DMT (Derjaguin-Muller-Toporov) and JKR (Johnson-Kendall-Roberts)[21,22].

The Sneddon, DMT and JKR elastic modulus models are based on the Hertz model and aim to expand and refine it. For example, Sneddon derived expressions for calculating Young's modulus when the AFM probe was approximated by such axisymmetric shapes as a cylinder, a cone, a paraboloid of revolution, etc. The DMT and JKR models allowed for the existence of adhesion forces between the probe and the sample. An important difference between these models is that in the first one it is believed that the adhesion forces act only outside the contact area, and in the second, on the contrary, only inside it. DMT is better suited for describing the contact of hard materials with poor adhesion, and the JKR model gives more accurate results when adhesive materials are in contact.

Existing methods for studying the mechanical properties of cells make it possible to assess the response of these objects to deformation, as well as to register the forces that cells create themselves. Among the active methods for measuring the mechanical characteristics of individual cells, despite the existing drawbacks, AFM looks very promising. It allows to study the morphology and mechanical characteristics of cells under physiologically adequate conditions with nanometer resolution.

2.2.2. Viscoelastic models for cell mechanics

Since cells do not behave elastically but viscoelastically, different models have been developed to describe the phenomena measured[10,23–29]. Viscoelastic models used are either

- Continuum models – cells are the sum of their parts
  - Standard linear solid
  - Fractional derivate models
  - Power law
  - Liquid drop
  - Standard linear viscoelastic
- Micro/nanostructural models – cell parts arrange in defined way and define properties
  - Tensegrity

2.3. Measurement of cell mechanical properties

Many methods for researching the mechanical properties of cells have been developed[30]. There are active and passive methods. The first one involves measuring the response of the cell to the action of deforming external forces (AFM, micropipette aspiration, optical or magnetic tweezers etc.). Passive methods measure the forces generated by the cell itself. They are mainly based on the use of a special non-toxic substrates (transparent or reflective) that change properties as reaction to forces from the cell.

Active methods usually provide information on the stiffness of cells, their elastic or viscoelastic (rheological) properties, while passive methods allow measuring the forces and corresponding tensile stresses that set cells in motion (cell traction forces, tensile stresses).

2.3.1. Micropipette aspiration

Among the options for measuring the mechanical characteristics of individual cells, the method of micropipette aspiration is widely used[31–33]. The working tool in micropipette aspiration is a pipette, which is a glass capillary, the inner diameter of which is less than the size of the measured object, i.e. cells. Usually, the diameter of

the inner channel of a micropipette does not exceed 10 μm. To measure the mechanical parameters of cells, the tip of the pipette is brought into contact with the object under investigation using a micromanipulator. A negative pressure is created in the pipette, under the action of which part of the cell is sucked into the microchannel (Figure 2-2).

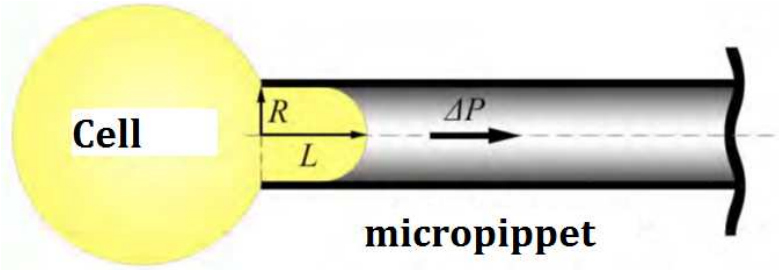

Figure 2-2. Principle of micropipette aspiration. A cell (shown as yellow circle) is sucked in by the negative pressure applied to a micropipette. The shape change of the cell is then monitored with a microscope and evaluated (e.g. using law of Laplace, where the difference in pressure is proportional to the surface tension and inversely proportional to the radius of curvature).

As a result, the cell undergoes deformation, by studying which it is possible to assess several mechanical quantities characterizing the object.

The micropipette aspiration method was used to study the mechanical properties of cells such as neutrophils, erythrocytes, chondrocytes, fibroblasts, endothelial, mesenchymal stem cells, cancer cells, dysentery amoeba and others. It was found that some types of cells behave like a drop of liquid enclosed in a shell, while others behave like an elastic solid. First of them, upon reaching a certain critical value of the pressure in the pipette, are rapidly sucked into it completely, while the others respond to an increase in the suction pressure only with greater deformation. The first type of cells includes blood cells (erythrocytes, neutrophils), and the second chondrocytes, endothelial, cancer cells.

In the model of a liquid drop, the cell is considered as a homogeneous Newtonian viscous liquid surrounded by a thin shell under constant tension, and in the model of an elastic solid - as a homogeneous solid.

2.3.2. Optical tweezers

Another method for studying the mechanical properties of cells are optical tweezers[34,35]. They are based on the effect of light pressure. As a result of reflection and partial or complete absorption of light by the body, a certain momentum is also transferred to the body, i.e. pressure is created. If the force of light pressure in optical

tweezers is large enough, it can make micro-sized particles move along the direction of propagation of the light wave. By moving the focus, you can control the position of the particles. The so-called gradient force forces the particle to move in the direction of increasing light intensity.

Using optical tweezers, erythrocytes, outer hair cells of the inner ear, embryonic stem cells, cardiomyocytes, osteoblasts and chondrocytes, yeast cells were examined. To implement the experiments in Figure 2-3 it is necessary that the spherical particles be firmly bound to the cell. To achieve reliable attachment of particles to a native object, they are coated with various substances that enhance the adhesion between the ball and the cell (antibodies, lectins, components of the extracellular matrix).

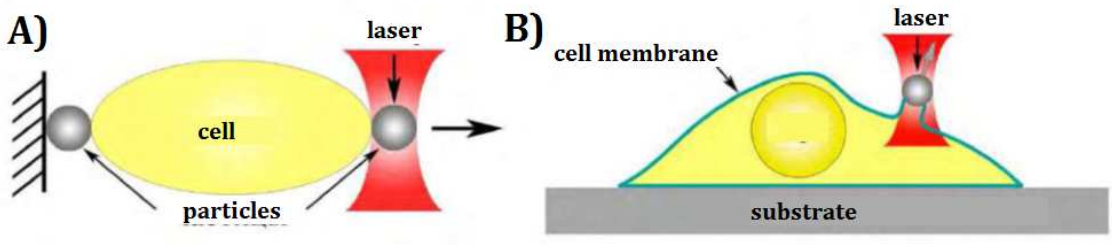

Figure 2-3. Schemes of experiments using optical tweezers. a) on stretching a single cell using optical tweezers (moving the focus to the right leads to displacement of the particle captured by the laser and stretching the cell) b) movement of the particle to the cell along the gray arrow leads to the formation of a membrane tubular structure (tether).

2.3.3. Atomic Force Microscopy

Atomic Force Microscopy is a technique of the family of scanning probe microscopy such as SNOM and STM. It works by measuring the interaction of a sharp needle (probe) with the surface of the object under study[36,37].

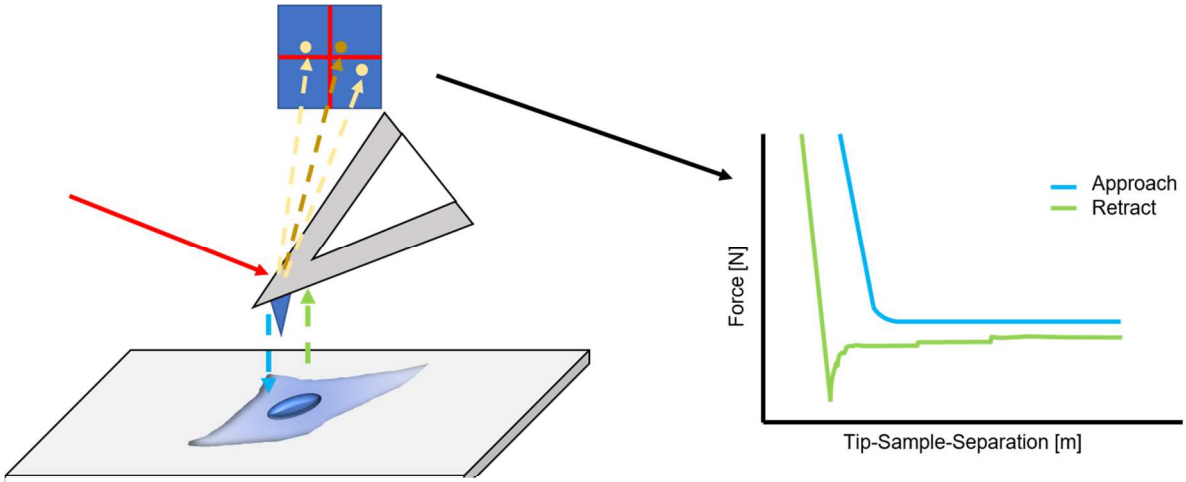

Figure 2-4. Working principle of an AFM. On the left-hand, a AFM cantilever can be seen with the laser focused on its backside. The laser is then reflected onto a photodiode and therefore the cantilever deflection is measured. On the right-hand side, a representative Force-distance-curve can be seen.

The principle of AFM work can be compared to such a human sense as touch, in which the properties of an object are obtained by touching it (see Figure 2-4). AFM can be thought of as a highly miniaturized human finger, thus small objects (in the range of nm to μm) can be studied in more detail, i.e. with high spatial resolution.

The operation of an atomic force microscope is based on the force interaction of the probe and its tip (cantilever) with the surface under investigation. The probe for AFM is an elastic arm, one end of which is rigidly fixed, and at the other end there is a needle, with the help of which the sample surface is probed (Figure 2-5). Most standard commercially available AFM probes are manufactured from silicon (Si) or silicon nitride (Si_3N_4). The shape of the console can vary. The most common are rectangular and triangular (or V-shaped) AFM probes. A typical cantilever is 100–200 μm long, 20–40 μm wide, and 0.5–1 μm thick. The length of the tip of a standard probe is several microns, and the radius of the tip is a few tens of nanometers.

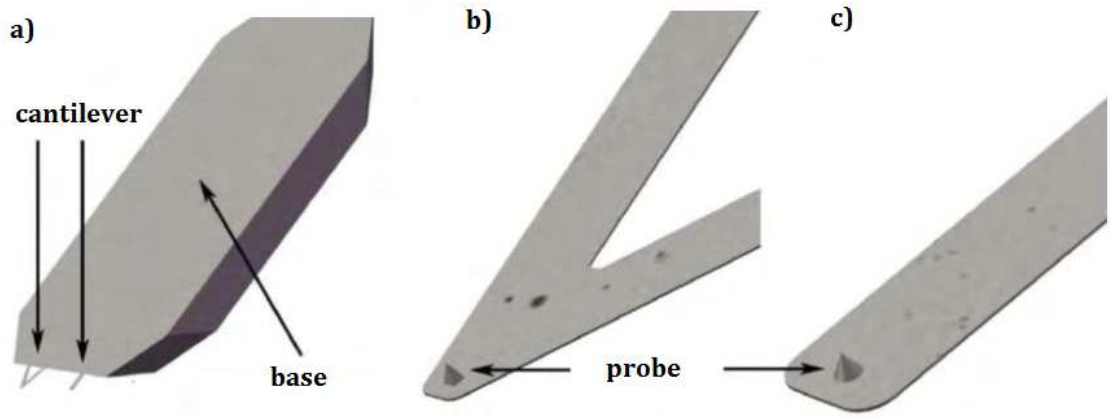

Figure 2-5. a) Schematic of the AFM probe sensor; b) triangular cantilever with tip; c) rectangular cantilever with tip.

In practice, forces of different physical nature act between the probe and the sample: van der Waals, electrostatic, capillary, magnetic, repulsion in contact, etc. Due to this, AFM makes it possible, in addition to studying the surface relief, to study material characteristics such as mechanical, electrical, magnetic properties of materials. In addition, AFM is actively used not only for studying, but also for modifying the surface of materials with nanometer resolution using force lithography.

Interpreting the nature of the force interaction between the probe and the sample can provide information about the mechanical characteristics of the sample.

Especially valuable is that due to the size of the AFM probe, the mechanical properties of the sample can be studied at the nanometer level.

The main method for studying mechanical properties in AFM is the (nano) indentation technique, i.e. deformation of the sample under load from the probe[38–40]. And the main source of quantitative information on the mechanical characteristics of a sample in AFM is the dependence of the force of interaction between the probe and the sample on the distance between them - the so-called force curves. The analysis of force curves allows quantitative determination of such mechanical parameters as deformation, stiffness, Young's modulus or viscoelastic properties. In addition, the curves can be used to measure the adhesion between the probe and the sample and the energy dissipation during indentation. In practice, there are several AFM methods based on the measurement and interpretation of force curves. Such operating modes are collectively referred to as force-distance curve-based AFM.

The working part of an atomic force microscope is a probe - a sensor with which the geometric and other parameters of the sample surface are measured. Mutual movement of the probe relative to the sample in the AFM is carried out using a piezoceramic scanner. Its action is based on the opposite piezoelectric effect - a change in the geometry of a body in response to an applied electric field. The use of piezo-materials in the construction of scanners of atomic force microscopes makes it possible to carry out precision movements, which, as a result, makes it possible to achieve a high spatial resolution of AFM images.

For imaging modes, the AFM probe moves over the sample, line by line recording the irregularity of the surface relief of the material under study. There are different scanning concepts depending on the design features of the atomic force microscope model. So, in some devices the sample is installed on the scanner and moves with it relative to the stationary probe (scanning with the sample). In others models the sample is static, and the piezo-scanner moves with a fixed probe on it (scanning with the probe). There are also AFM systems in which both scanning options are combined. As a result of force interaction with the investigated surface during AFM scanning, the cantilever bends.

AFM calibration to measure Force-distance curves

As described above, the cantilever of the AFM bends due to interactions between the tip and the sample. The bending of the cantilever can be recorded in various ways. However, the most widespread in AFM is the optical detection system. With this method of registering cantilever deflections, a laser beam falls on the rear mirror side of the probe console above the needle, which, being reflected, hits a four-section photodiode. As a result, an electric current is generated in the detector, the total signal being the sum of the components arising in the individual segments. The bending or deflection of the cantilever (Z_c) is proportional to the strength of interaction following

$$F = k_c \times Z_c \qquad \text{Eq. 5}$$

Note that k_c is the spring constant of the cantilever. Initially, when the cantilever is in an unbent state (far from the sample surface), the detection system is adjusted so that, after being reflected from the probe beam, the laser beam hits the center of the photodetector. In this case, the difference signal between the two upper and two lower sections will be equal to zero. The bending of the cantilever will lead to a displacement of the spot from the laser beam relative to the center of the photodiode and a proportional change in the electrical signal (voltage, ΔU or current, ΔI) on the photodetector.

Prior to measurements, one needs to calibrate the used cantilever[41]. This is done to determine how much bending (as length) corresponds to how much change in voltage. Then, by usage of the thermal motion of the cantilever using the first free vibration mode, one can calculate the stiffness of the cantilever. This is done according to the equipartition theorem

$$k_c = \frac{k_b T}{\langle {Z_c}^2 \rangle} \qquad \text{Eq. 6}$$

with the term $\langle {Z_c}^2 \rangle$ as the mean square deflection of the cantilever, k_b as the constant of Boltzmann, and T as the temperature of the system. Prior to each set of measurements, cantilevers need to be calibrated.

3. Materials and Methods

3.1. Cell Culture

3.1.1. Cell Culture Routine

Human umbilical veins endothelial cells (HUVEC) were used in this Master Thesis to study the mechanical properties of endothelial cells. These cells have only minor requirements regarding the used media, as well as the passaging and maintenance protocol, leading to quite easy routine handling. The cell line was provided kindly by Dr. Spela Zemljic-Jokhadar from the Medical Faculty of the University of Ljubljana.

All the cell culture protocols were done under sterile conditions under a laminar hood (Herasafe KS12 from Thermo Fisher Scientific). In addition, materials used (including pipettes, tubes and flasks, all from Sarstedt, Germany) were either purchased sterile or sterilized by autoclavation. As culture medium, sterile filtered DMEM with GlutaMax™ and high glucose (4.5 g/L) was used. The medium was supplemented with 10% fetal cow serum (FCS/FBS) and 1%penicillin/streptomycin (all purchased from Gibco®, Thermo Fisher Scientific). Cells were stored frozen in the gas-phase above liquid nitrogen at temperatures between – 140 and -180 °C in the same medium as described above with the addition of 10% DMSO. After thawing, cells were resuspended in DMEM and plated on a T75 cell culture flask (Sarstedt, Germany) at 37 °C with 5% CO_2 and 95% humidity in an incubator (Heraeus BBD 6220, Thermo Fisher Scientific). After approximately 48 hours, a confluence of 70 – 80% was reached (checked by light microscopy). Therefore, cells were passaged every 48 hours 1:5. A micrograph of the cells can be seen in Figure 3-1.

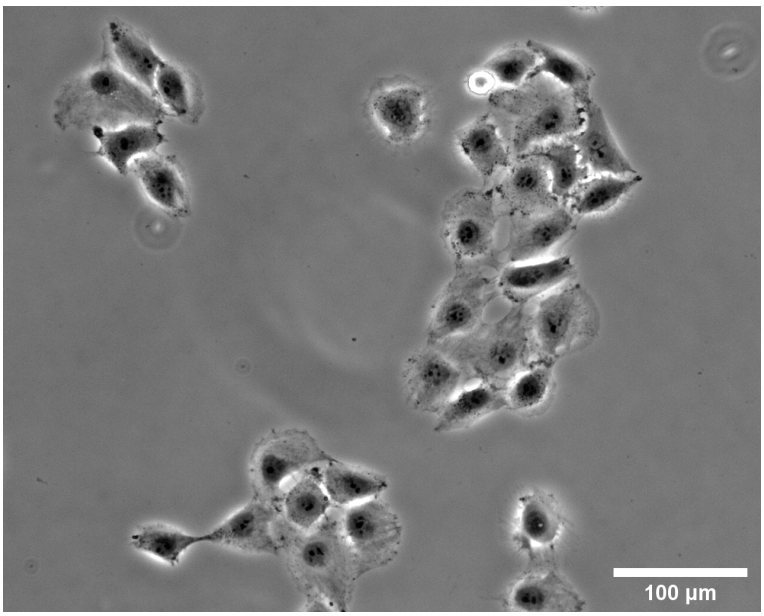

Figure 3-1. Optical micrograph of HUVECs grown for 24 hours on glass slide in DMEM + 10 FBS + 1% PenStrep. Image was done in Phase 2 with a 20x air objective.

For passaging, cells were taken from the incubator and checked by microscopy. They were then washed one time using phosphate buffer (1X PBS, pH 7.4, also from Gibco). After removal of the buffer, 2 mL of TrypLE™ was added and cells were incubated from 5 – 10 min in the incubator. The solution was then diluted with 5 mL of the above described medium. This suspension was centrifuged at room temperature at 1200 rpm for 5 minutes using a benchtop centrifuge equipped with a SX4750A rotor (Allega™ X-12R centrifuge, Beckman Coulter Life Sciences, USA). The pellet was dissolved in 5 mL medium, 1 mL of this suspension was put into a T75 flask. Then, 10 mL of the medium was added, and the culture flask was put into the incubator.

To later study mechanical properties and to determine cell viability, cells were counted routinely. This was done using an automated cell counter (Countess ® Cell Counter). Each time, 10 µL of the cell suspension prepared as described above was stained using 10 µL of trypan blue (0.4 %, Thermo Fisher Scientific, US). This stains only dead cells. A cell viability of about 90% was reached all the time using the above described culture conditions. A HUVEC culture was only used until approximately 35 passages.

3.1.2. Sample preparation for Atomic Force Microscopy

HUVECs were grown as described above. They were then trypsinized for 5 to 10 min. Prior to cell seeding, thin, circular glass slides (radius of 12 mm, Menzel Gläser,

VWR, Germany) were washed in EtOH. They were then dried in nitrogen. Oxygen plasma (Gala Instruments GmbH, Germany) was used for 20 s with approximately 60 W and a flow rate of 100 cm^3/min to clean and activate the surface, making it more hydrophilic. Immediately after cleaning, the slides were put into 1X PBS at 37 °C to keep the activation. Then, 1 mL of cell suspension with a concentration of 40,000 cells per mL was added to the slide and diluted with 2 mL of medium. These slides were incubated with the cells for 24 hours at 37 °C. Cells were then washed thrice with PBS and 2 mL of CO_2 independent Leibovitz media without any supplements was added.

3.2. Cantilever preparation

For measurements using a tip, a DNP-S cantilever (Bruker) was used. This is a triangular cantilever with a four-sided pyramidal tip. The schematics of the cantilever and the tip can be seen in Figure 3-2. Of the chipset, cantilever B was used with a nominal spring constant of 0.12 N/m and a resonance frequency of 23 kHz. The cantilevers were cleaned with EtOH and 30 min of UV/O cleaning prior to

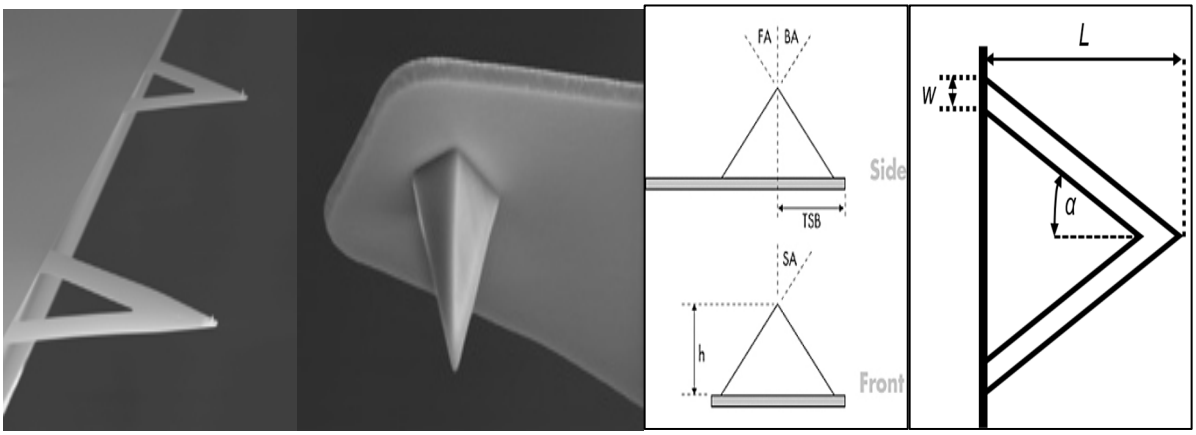

Figure 3-2. Scanning Electron Microscopy image of a cantilever chip (left) and zoom-in onto the tip region (next to it). The two images on the right show the schematic proportions of the cantilever.

measurements.

To prepare cantilevers with particles, tipless NP-0 cantilevers were used (Bruker). They were first UV/O cleaned for 30 min. Then, a silica particle with a radius of 10 µm was glued onto them using a UV-curable glue (Norland optical adhesives). For this process, first 2 glass slides were plasma cleaned. Then the glue was put onto on glass slide and spread until only small droplets remained. The cantilever was mounted on the AFM and brought into contact with the glue for 2 s. Thus, glue was spread on the cantilever. Then, the glass slide was switched to a new clean on and 300

µL of a 1:1000 dilution of the 10 µm diameter particles were added. A drop of water was added to the cantilever, and the cantilever was then brought into the liquid. Then, a particle was approached carefully, and the cantilever pushed gently on to the particle with a force of 2 – 10 nN for 5 s. Repositioning using the x/y movement of the piezo was done to place the particle central. The cantilever was then retracted and

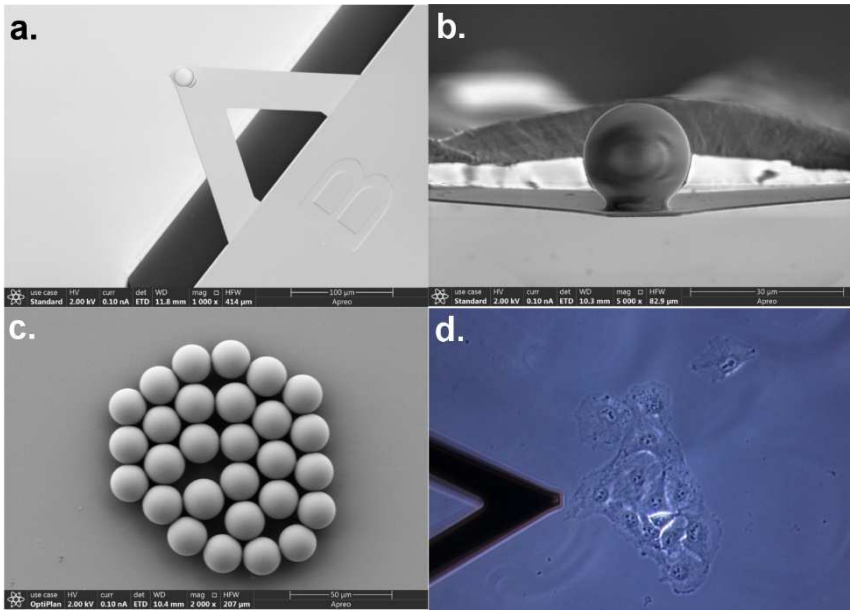

Figure 3-3. Scanning Electron Microscopy image of a cantilever chip with a particle glued to it (a). In (b) the same cantilever can be seen from a side view. Figure (d) shows a cantilever on top of cells.

the glue pre-hardened using short-wave UV light. After that, the cantilever was dismounted, cured with short wave UV light for 45 min and cured over night at 60 °C. Before use, cantilevers were cleaned with UV/O for 30 min. Figure 3-3- shows a cantilever with a particle glued to it.

3.3. Atomic force microscopy

For mechanical property measurement of cells, a JPK Nanowizard III AFM (JPK instruments AG, Germany) was used. The AFM has a z-piezo rang of 15 µm and a x and y range of 50 µm. For cell measurements, a CellHesion module was used, increasing the z-range up to 100 µm. This decreases the reaction time of the piezo crystal. A Biocell® sample holder was used, to enable measurements in liquid media and at 37 °C. The backside of the glass slides with cells grown for 24 hours on them was wiped with a tissue to remove residual salts; the slide was then added to the sample stage. 600 µL of the medium was added and the sample was left to equilibrate for 30 min.

For measurements the cantilevers as described above were fixed on the AFM with a metal spring. First, the laser point was focused on the back-end region of the cantilever and the deflection signal was maximized. Spring constants of approximately 0.12 N/m ± 0.05 were measured.

The AFM is combined with a Axio Observer Z1 inverted microscope (Carl Zeiss GmbH, Germany). We used a 20x air objective, measured with a CCD camera (DFX 31AF03). Figure 3-4 shows an example of HUVECs grown for 24 hours below a cantilever.

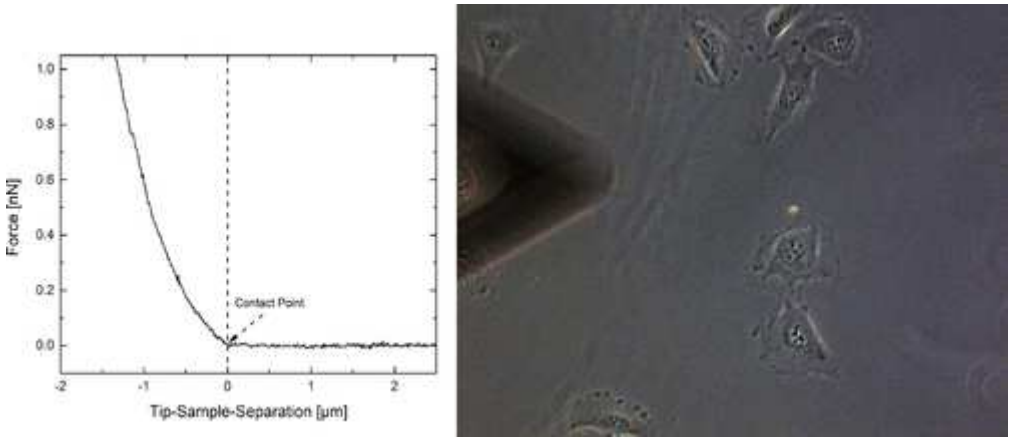

Figure 3-4. (Left) Force-distance curve of the indentation of cell using a pyramidal indenter. (Right) Cells grown for 24 hours on glass slide, cantilever can be seen to the left of the image.

3.3.1. Force Spectroscopy Method

For both used cantilevers (pyramidal tip with nominal radius of below 20 nm and 10 µm diameter silica particle), we used similar measurement set-ups. The cantilever was lowered to a region of cells and measurements on glass were performed. Then the cantilever was moved above the nuclear region of a cell. On each cell, 5 measurements of the different measurement settings were done. We varied the loading to values of 0.5, 5 and 10 µm/s. This is a loading rate regime normally used for cell mechanical studies. As maximum load (maximum force) we used values of 1 nN and 2.5 nN. At least 5 cells were measured. We optimized the curve length as well as the sample number according to the measurement settings. In between cell measurements, the glass was indented to ensure that the cantilever didn't carry any cell fragments.

3.3.2. Data analysis

Contact Point and Baseline definition using JPK SPM software

As described above, a typical indentation experiments have a baseline and a contact region of the curve. Therefore, it is important to determine the baseline and the contact point. In this thesis, both were determined by hand using the software provided by the manufacturer (JPK SPM, JPK Instruments, Germany, 6.1.159).

Figure 3-5 shows the four-step procedure to work on raw Force-Distance curves before they can be extracted. Note that these files already have the calibration inside (therefore the y axis is in force units). Curves where inspected visually, and outliers were removed. The steps are done as described in the JPK SPM User Manual. The steps include the following

a. A raw Force-Distance curve is loaded into the software. In red one can see the approach/indentation segment, in blue the retraction. A hysteresis is visible indicating that cells are not ideally elastic. The baseline is clearly visible.
b. The baseline is determined by choosing enough of the measuring points of the line before contact (no slope means no interaction). Then the curves are tilted by the baseline. The difference between the two baselines (red and blue) results from instrument drift.
c. The contact point is defined automatically by the software. Then it is adjusted by eye as the point with the first significant deviation from zero-point slope.
d. Finally, the x-axis is corrected for the cantilever bending (where the cantilever deflection is subtracted from the piezo height). This is needed to get the real deformation.

The last step was done because in Force-distance measurements with the AFM, the distance between tip and sample is measured as

$$D = Z_p - (\delta_c + \delta_s), \qquad \text{Eq. 7}$$

With the measured parameters being Z_p, the position of the piezo and the sum of both deformations δ_c (deflection of the cantilever) and δ_s (deformation of the sample). Since the cantilever is an ideal Hookean spring, the Force is connected to the deformation via the spring constant. Therefore, in contact with the sample (assuming no piezo displacement), the deformation of the sample is

$$\delta_s = Z_p - \delta_c = Z_p - \frac{F}{k_c}. \qquad \text{Eq. 8}$$

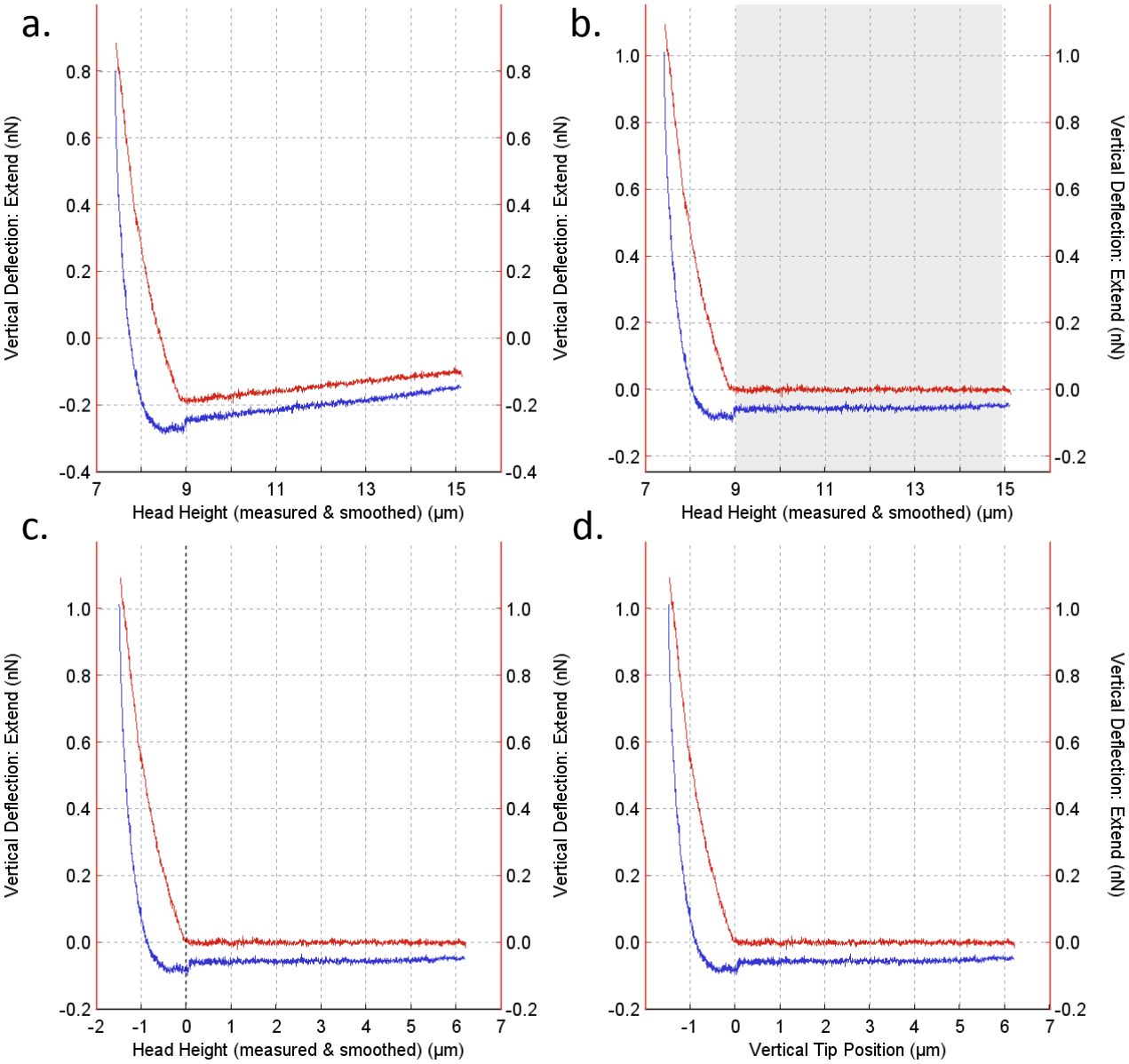

Figure 3-5. Correction steps of Force-distance-curves. (a) Raw Force-distance-curve, in red the approach and in blue the retract can be seen. (b) Baseline correction of the curve and tilting of the baseline. (c) Definition of contact point. (d) Correction for the bending of the cantilever.

Curve Extraction and Import into Origin Pro

Further data analysis was performed in Origin Pro 2018 (9.5.1.195, OriginLab Corporation). For this, after curve processing, the Force, indentation and time segments of the approach curves were extracted as ASCII-files using a batch routine. Then curves were imported automatically into Origin Pro using a short self-written command.

Plotting of Force-distance curves

Then, Force-distance curves were plotted of all pooled data-sets (pooled according to measurement settings) Figure 3-6 shows a single and all the

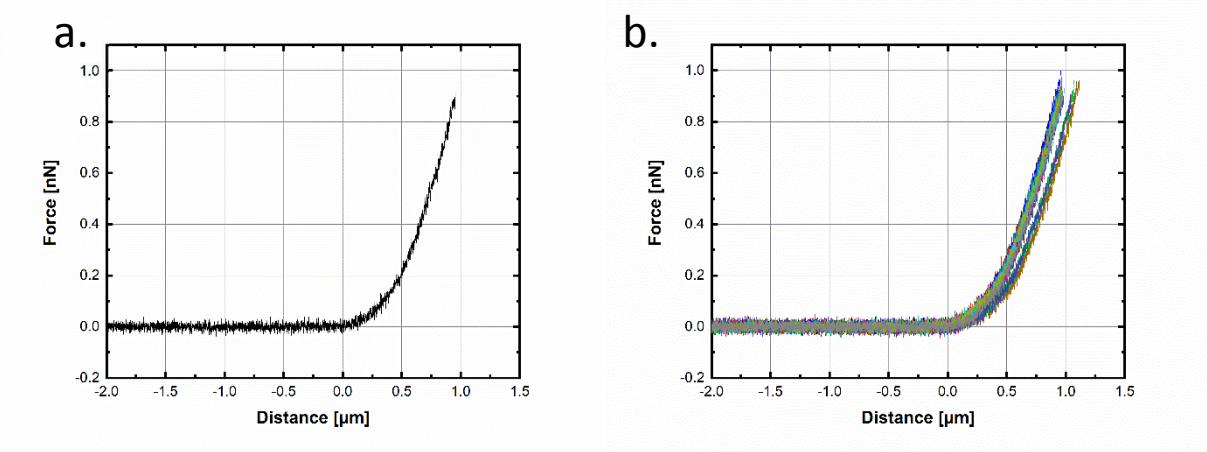

Figure 3-6. (a) Single F-d-curve after full correction. (b) Multiple F-d-curves for the same settings showing that the measurements look similar and data can be pooled.

measurements performed for the settings 5 µm/s, maximum force of 1 nN and with a 10 µm silica particle as indenter.

Plotting of Force-δ^i- curves

In the next step, we calculated either the square of the indention (δ^2)for pyramidal indenters or the $\delta^{3/2}$ for spherical indenters and then plotted the force against the determined values. Examples for loading rates of 5 µm/s and a maximum force of 1 nN can be seen for both pyramidal tips and particles in Figure 3-7. These plots are then used to determine the Young's Modulus by fitting linear functions to different regions of the plots.

Determination of apparent depth dependent stiffness

In a next step, the apparent, depth dependent stiffness was determined from the force-distance-curves. The stiffness of a sample corresponds to the slope of the F-δ-curve. This is an extensive property, expressed in units N/m, which depends on the boundary conditions. Thus, it does depend on the geometry of the contact (pyramidal tip vs. spherical particle), values derived cannot be compared without some correction factors. The measured stiffness is defined as

$$k_m = \frac{\Delta F}{\Delta \delta} \qquad \text{Eq. 9}$$

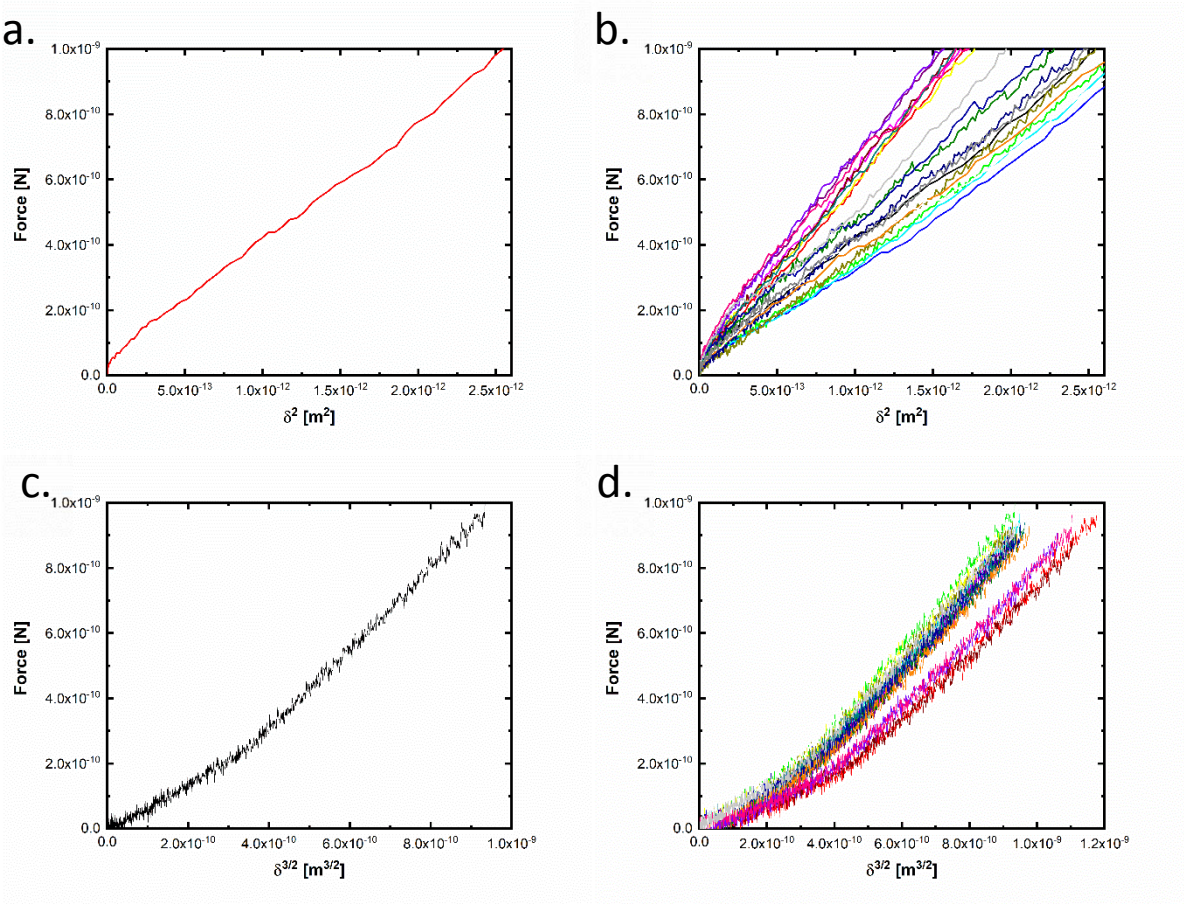

Figure 3-7. (a) Force-δ^2-curve for a single curve performed with a pyramidal tip cantilever and (b) all the curves for the same measurement settings. (c) Force- $\delta^{3/2}$-curve for a single curve performed with a spherical particle and (d) all the curves performed for such measurement settings.

And sample heterogeneities as well as contact geometry differences are visible as changes in the slope. To determine the stiffness of the sample from the measured stiffness (k_m), the system is modelled as two springs in series, leading to

$$\frac{1}{k_m} = \frac{1}{k_c} + \frac{1}{k_s} \qquad \text{Eq. 10}$$

With the stiffness of the cantilever (k_c) being known and the measured stiffness being a fitting property. Therefore, the stiffness of the sample (k_s) is

$$k_s = \frac{k_m k_c}{k_m + k_c} \qquad \text{Eq. 11}$$

The fittings of the stiffness were performed over different indentation depths of Force-distance-curves being δ of 0 – 200 nm, 200 – 400 nm and 400 – 800 nm. This indentation depth was used since in theory it should correspond to different parts of the cell being indented (membrane/cortex vs cytosol vs nuclear region). The pressure distribution of a tip differs from that of particle (considering contact areas) differs, leading to higher indentations for tips at the same force compared to that of particles.

Therefore, reciprocal linear fittings of δ-Force-curves were performed over different force ranges from 0 – 200 pN, 200 – 400 pN, 400 – 600 pN and 600 to 800 pN.

Determination of Young's Modulus

A linear elastic Hertzian contact model was used with a Sneddon extension. Of this model, the general relation of Force to Indentation is

$$F(\delta) = c \times \delta^n \qquad \text{Eq. 12}$$

Where c is a constant that depends both on material properties (such as the Poisson ratio) and contact geometry, and the exponent n depends on the indenter geometry. For a pyramidal indenter, the Young's Modulus can be determined as

$$F = \frac{E}{1-\upsilon^2}\frac{\tan(\alpha)}{\sqrt{2}}\delta^2, \qquad \text{Eq. 13}$$

With (E) the Young's Modulus, (ν) the Poisson ratio (set to 0.5 assuming incompressibility, (α) the opening angle of the pyramid). For a parabolic indenter (with the assumption of not deep indentations, which is a simplification of spherical contact), the relationship is

$$F = \frac{4}{3}\sqrt{R_c}\frac{E}{1-\nu^2}\delta^{3/2} \qquad \text{Eq. 14}$$

where (R_c) is the indenter radius (for low indentations). From both equations by plotting a curve of the force against δ^i, with i = 2 for the pyramid and i = 3/2 for the particle, one should get a straight line if the assumptions of linear elasticity are true. Fitting such a curve with a linear function leads to solutions for getting the Young's Modulus, which is for the pyramid then

$$E = \frac{(1-\nu^2)\times\sqrt{2}}{\tan\alpha}\frac{\Delta F}{\Delta\delta^2} = \frac{(1-\nu^2)\times\sqrt{2}}{\tan\alpha}S \qquad \text{Eq. 15}$$

And for the spherical particle

$$E = \frac{3}{4}\frac{1-\nu^2}{\sqrt{R_c}}\frac{\Delta F}{\Delta\delta^{3/2}} = \frac{3}{4}\frac{1-\nu^2}{\sqrt{R_c}}S \qquad \text{Eq. 16}$$

Both fittings were done over different ranges of the respective curves and the fitting quality for the different ranges was evaluated.

4. Results and discussion

In this work the influence of loading rate, maximum load and indenter geometry on the measurement of mechanical properties of HUVECs using AFM was evaluated. As a first step, the generated Force-Distance-Curves were compared for the tips and the particles.

4.1. Influence of loading rate and maximum force on F-δ-curves

In Figure 4-1, the different F-δ-curves for measurements done with a pyramidal tip can be seen. The left row always shows the measurements with a maximum force of 1 nN, while the right row shows the ones with 2.5 nN. Some first interpretations can be made: Apparently an increase in loading rate leads to a lower maximum indentation. This can be interpreted as the cells appearing stiffer. For the curves done at the same parameters, similar curve shapes are seen. In addition, curves made at higher speed appear to have less curve to curve variation. A similar conclusion can be said for the curves performed using a 10 µm silica particle, here the results can be seen in Figure 4-2.

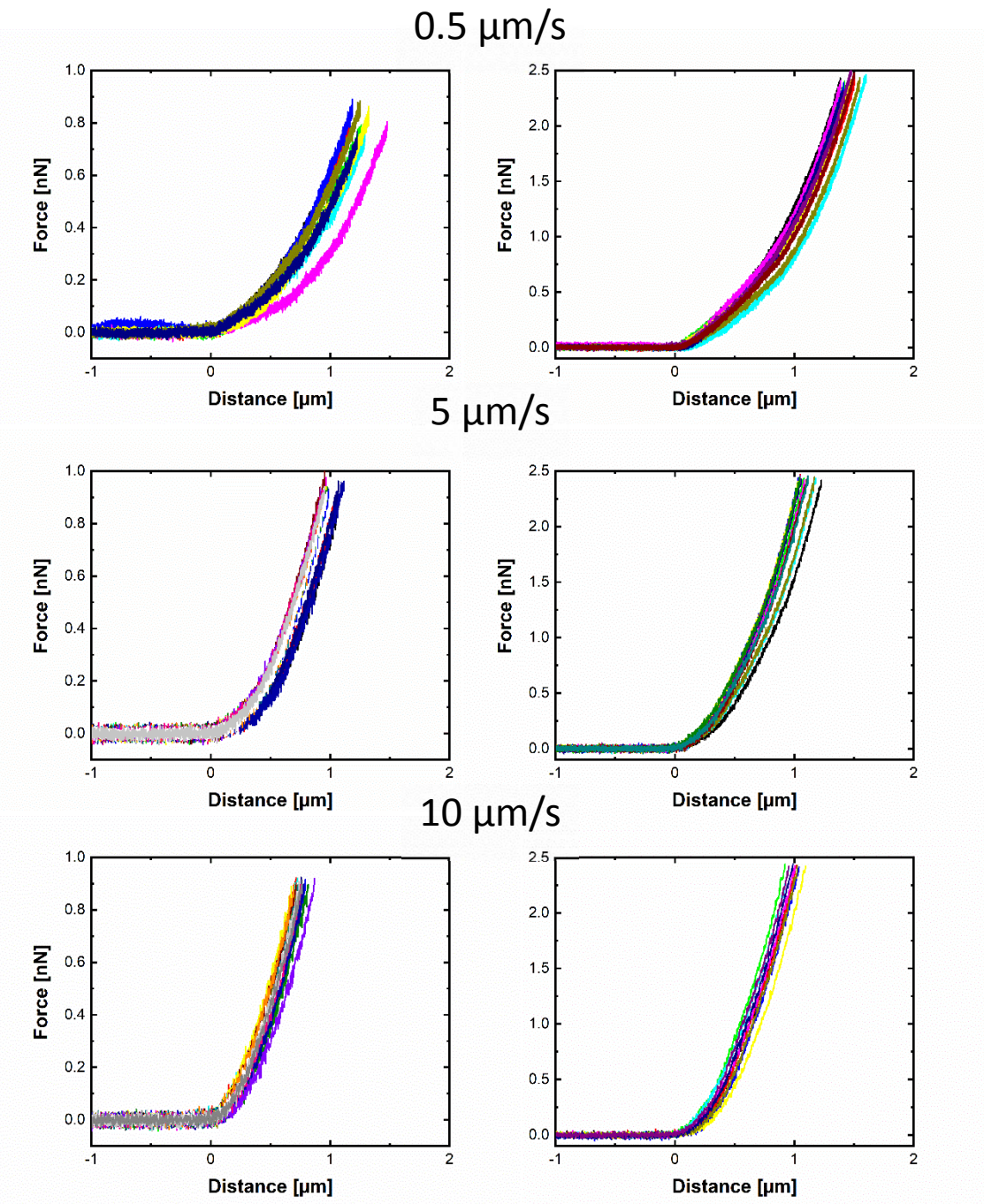

Figure 4-1. Force distance curves of measurements performed using a pyramidal tip as an indenter. Top row shows those done at 0.5 µm/s (1 nN left and 2.5 nN right), middle show shows those done with 5 µm/s (1 nN left and 2.5 nN right), and the bottom row shows those performed using a rate of 10 µm/s.

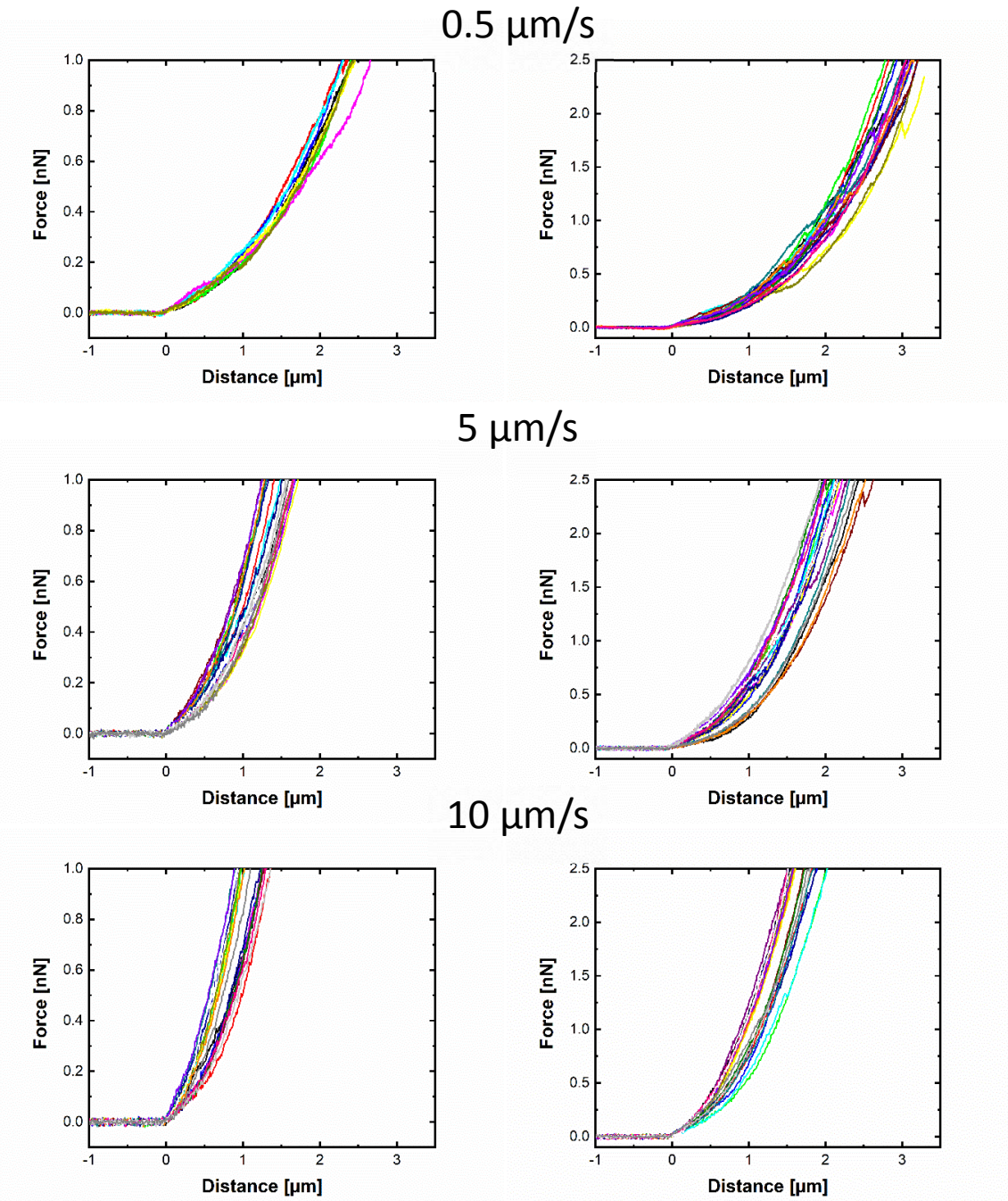

Figure 4-2. Force distance curves of measurements performed using a particle as an indenter. Top row shows those done at 0.5 µm/s (1 nN left and 2.5 nN right), the middle row depicts those done with 5 µm/s (1 nN left and 2.5 nN right), and the bottom row illustrates those performed using a rate of 10 µm/s.

4.1.1. Comparison of measurements done with tips and particles

The comparison of Figure 4-1 and Figure 4-2 shows some interesting things: First, for the particle sometimes the technically wished maximum force was not reached. This can be explained partly by higher hydrodynamic drag on the cantilever

due to the colloidal particle. This is a force that opposites the movement of the cantilever in the aqueous medium. Secondly, curves for the particle seem to have less deviation in between the curves. Thirdly, at the same force and loading rate, the indentation is lower for the particles. Considering Hertzian mechanics, this make sense, since more force is needed to reach the same indentation for particles. Figure 4-3 shows a comparison of the maximum indentation depth for both particles (left) and tips (right). As describe before, the deviation of values appears to be lower for the particle. Also, already it is visible that the indentation depends non-linearly on the maximum force.

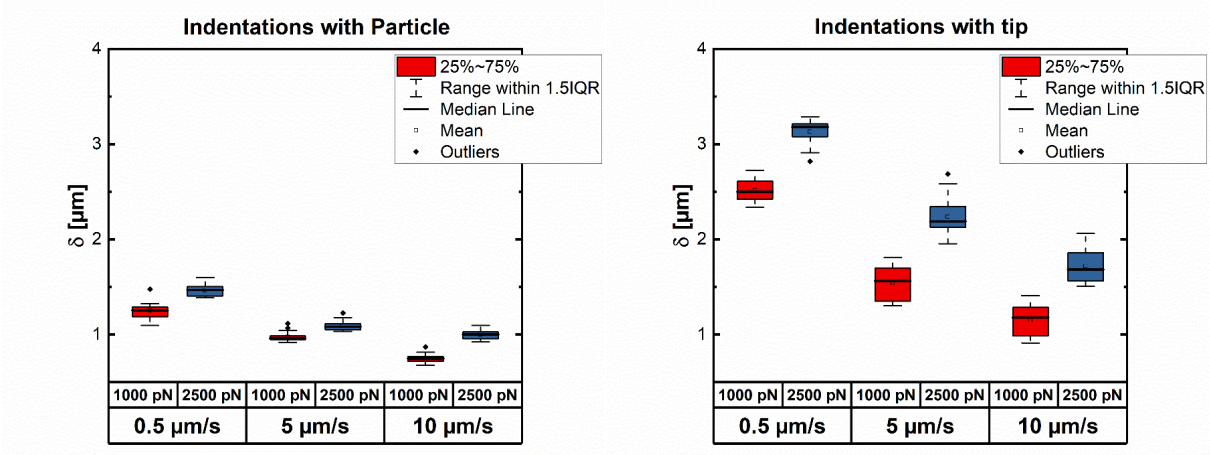

Figure 4-3. Maximum indentations at the given measurement settings for particle measurements (left) and pyramidal tip measurements (right). In red, measurements using 1 nN maximum force are shown while in red it is the ones with 2.5 nN. All the used loading rates are shown.

4.2. Slope of Force-Distance curves to determine sample stiffness

In a next step, the slope of the force-distance curve was evaluated as a measure of stiffness. As already discussed above, only indentations for similar geometry and for similar indentation depths can be compared. The reason is the non-linear increase in Force, since $F \propto \delta^i$.

4.2.1. Slope for tips in F-δ-curves increases with loading rate

Figure 4-4 shows an example of the multiple linear fittings performed for a Force-distance curve using a tip. The regions that were fitted are indentations of 0 to 200 nm, 200 to 400 nm and 400 to 800 nm. As can be seen by the adjusted R^2, the

fittings work rather well. Again, one must note that fittings of different indentations depths are only comparable, when taking into account the quadratic increase of force with indentation.

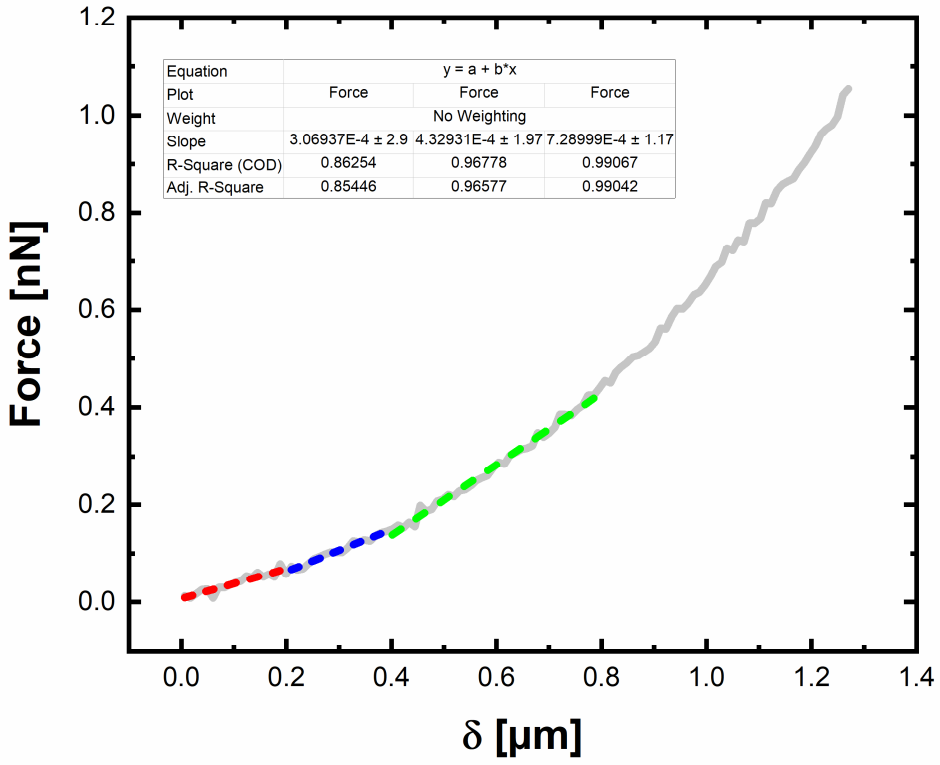

Figure 4-4. Force distance curve of a measurement performed with a tip and a loading rate of 5 µm/s and a maximum force of 1 nN. The grey line indicates the measurement while the dashed lines show a fitting over a range of 0 to 200 nm (red), 200 to 400 nm (blue) and 400 to 800 nm (green). The fitting performed was a linear fitting.

The fittings for the different loading rates were carried out, furthermore, the results were compared. Note that the values for measurements with a maximum force of 1 or 2.5 nN were pooled. Figure 4-5 shows the results of the slope fittings, here corresponded to as k_m.

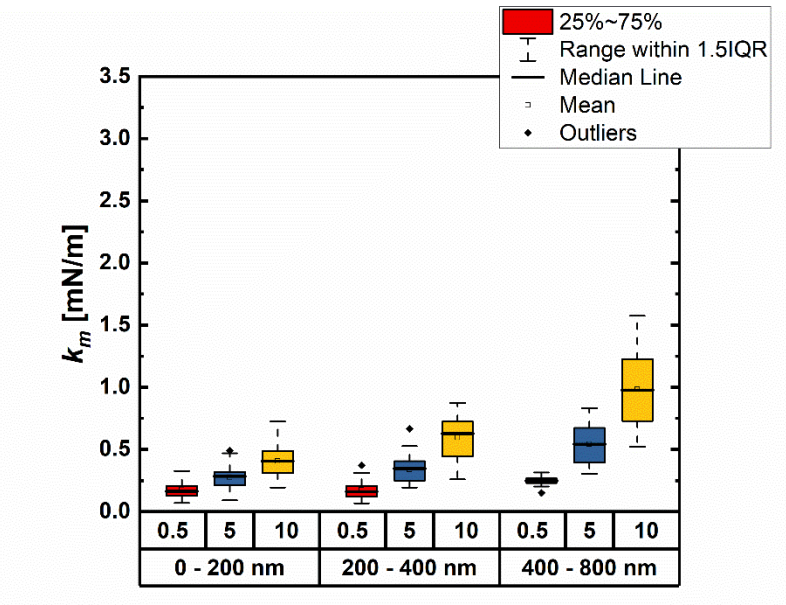

Figure 4-5. Calculated measured stiffness values from Force-distance curve fittings over ranges of 0 to 200, 200 to 400 and 400 to 800 nm for the different loading rates. Note that the measurements for 1 and 2.5 nN were pooled.

As can be seen, the increase in loading rate also leads to an increase in the slope. The increase appears to be roughly linear. This means that the apparent stiffness of the sample appears to be increasing with loading rate. Looking at the same loading rate, the slope increases following roughly a polynomial function of second order with respect to the indentation, thus following what is expected considering elastic contact with a pyramidal indenter. In Table 4-1, the determined values for the sample (the cell) stiffness in mN/m can be found.

Table 4-1. Sample (cell) stiffness in mN/m for various loading rates and indentation regions using pyramidal tips as indenters.

	0.5 µm/s	**5 µm/s**	**10 µm/s**
0 – 200 nm	0.17 ± 0.01	0.28 ± 0.01	0.40 ± 0.02
200 – 400 nm	0.17 ± 0.01	0.34 ± 0.02	0.60 ± 0.03
400 – 800 nm	0.25 ± 0.01	0.54 ± 0.03	0.98 ± 0.04

4.2.2. Slope for particles is higher and increases differently

In a next step, we performed similar fittings as described above for the measurements performed with particles. Figure 4-6 shows such segmented linear fittings for a F-δ-curve measured with a 10 µm diameter silica particle, a loading rate of 5 µm/s, and a maximum load of 2.5 nN.

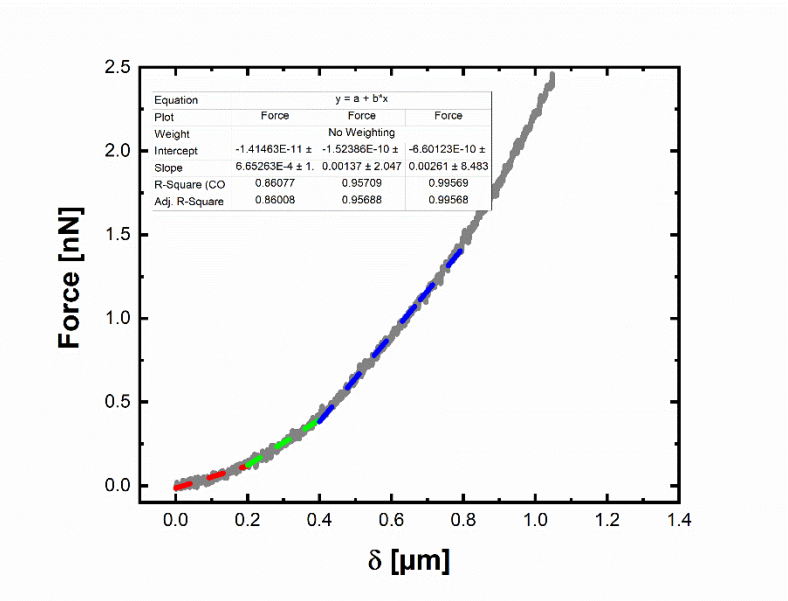

Figure 4-6. Force-distance curve of a measurement performed with a particle and a loading rate of 5 µm/s and a maximum force of 1 nN. The grey line indicates the measurement while the dashed lines show a fitting over a range of 0 to 200 nm (red), 200 to 400 nm (blue) and 400 to 800 nm (green). The fitting performed was a linear fitting.

As before the previous case, the fittings are reasonably good. Then, as a next step, this evaluation was done for all the measurements made with the particles. The measured stiffness can be found in Figure 4-7. Note, that only measurements at the same indentation range are comparable without any further considerations.

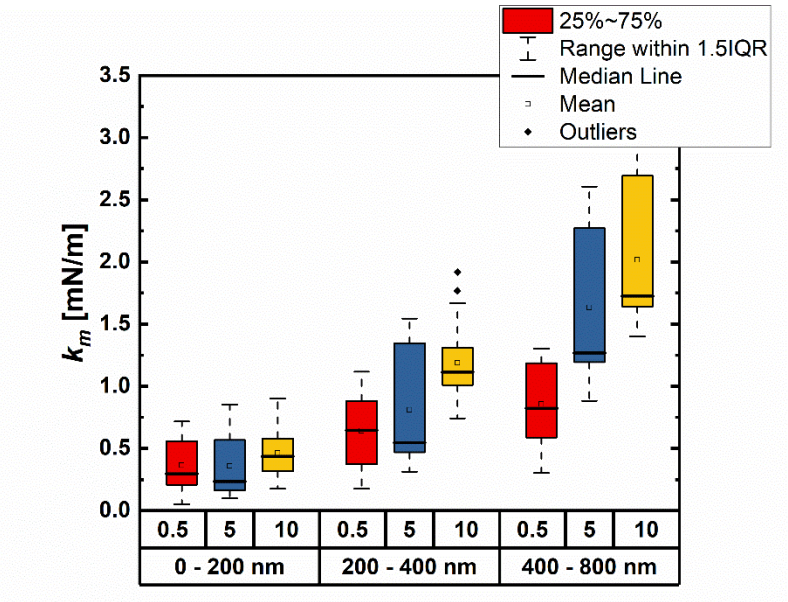

Figure 4-7. Calculated measured stiffness values from Force-distance curve fittings over ranges of 0 to 200, 200 to 400, and 400 to 800 nm for the different loading rates performed with a particle. Note that the measurements for 1 and 2.5 nN were pooled.

Interestingly, there seems to be no real difference between loading rates at very small indentations of 0 to 200 nm. For higher loading rates, an increase with the

loading rate is visible. The increase of the slope with indentation range for the same follows a rough scaling of 3/2. Finally, again the sample stiffness for the loading rate and indentation rate was calculated. They are shown in Table 4-2.

Table 4-2. Sample (cell) stiffness for various loading rates and indentation ranges using particles as indenters.

	0.5 µm/s	5 µm/s	10 µm/s
0 – 200 nm	0.36 ± 0.05	0.36 ± 0.04	0.46 ± 0.03
200 – 400 nm	0.64 ± 0.07	0.80 ± 0.08	1.18 ± 0.05
400 – 800 nm	0.85 ± 0.08	1.61 ± 0.10	1.98 ± 0.11

Taking now into consideration the scaling laws corresponding the different geometries, it seems reasonable, that the slope increases differently for the different geometries (approximately doubling for the tip and quadrupling for the particle measurements).

4.3. Slope of indentation-Force curves probed at different force ranges

As next evaluation step, d-F-curves were plotted and linear fittings were performed over a range of 0 to 200 pN, 200 to 400 pN, 400 to 600 pN and 600 to 800 pN. The reason is that maybe for the similar force range, the slope values for tips and particles are comparable.

4.3.1. Slope for tips in δ-F-curves decrease with loading rate

In Figure 4-8, an indentation-Force curve for a measurement performed with a tip and a loading rate of 5 µm/s and a maximum force of 1 nN can be seen (this is the inverse of a Force-distance-curve). The red, blue, green and orange line are the respective linear fittings. The fitting values can be seen in Table 4-3

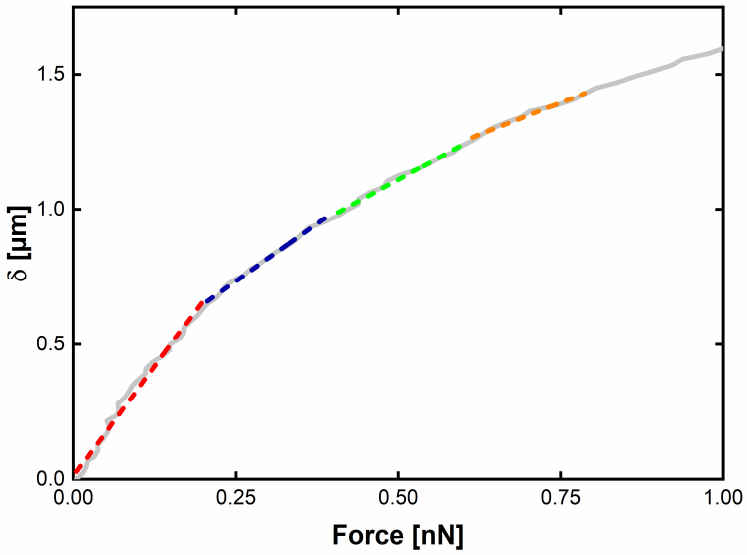

Figure 4-8. Indentation-Force curve measured for a pyramidal tip at a loading rate of 5 µm/s and a maximum force of 1 nN. The dashed lines show linear fittings to different curve segments of 0 to 200 pN (red), 200 to 400 pN (blue), 400 to 600 pN (green), and 600 to 800 pN (orange).

Table 4-3. Slopes from indentation-forces curve fittings for the curve shown in Figure 4-8 performed with pyramidal indenter.

Range (pN)	0 – 200	200 – 400	400 – 600	600 – 800
Slope	3250.1 ± 83.9	1685.9 ± 34.4	1314.9 ± 46.9	934.8 ± 47.2
Residual Sum of Squares	1.931E-14	7.0746E-16	1.1702E-16	4.8488E-16
R-Squared	0.98167	0.9946	0.9862	0.98248
Adj. R-Squared	0.98102	0.99419	0.98494	0.97998

Not surprising, the change in indentation over force decreases the higher the force range is. Again, the fittings seem to perform quite well. To evaluate this behavior, such fittings were performed for all curves with tips, again pooling values made for maximum forces of 1 and 2.5 nN.

This evaluation can be seen in Figure 4-9 The measured slope decreases both with indentation rate as well as with increasing force segment. The decrease with indentation rate is non-linear. In contrast to the values determined for the different indentation ranges, for the force ranges there is always a change in the slope. Table

4-4 shows the mean values with the corresponding standard error of the determined values in m/mN.

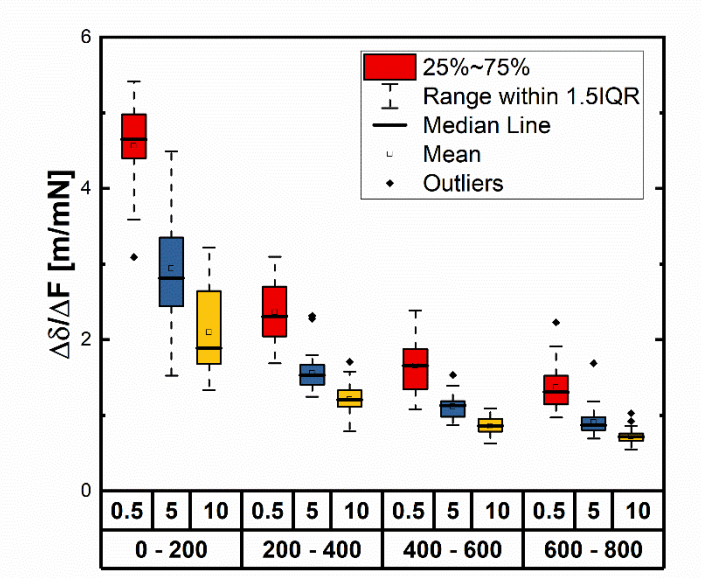

Figure 4-9. Fitted slopes for indentation-force curves in m/mN. In red, the values for loading rates of 0.5 µm/s are shown, in blue for 5 µm/s, and in yellow the ones for 10 µm/s. The measurements were performed with a tip.

Table 4-4. Slopes from various region fittings of δ-F-curves performed with a pyramidal tip at different loading rates in m/mN.

	0.5 µm/s	5 µm/s	10 µm/s
0 – 200 pN	4.57 ± 0.12	2.94 ± 0.11	2.10 ± 0.08
200 – 400 pN	2.36 ± 0.09	1.56 ± 0.04	1.21 ± 0.03
400 – 600 pN	1.66 ± 0.07	1.12 ± 0.02	0.86 ± 0.02
600 – 800 pN	1.37 ± 0.06	0.91 ± 0.03	0.72 ± 0.01

4.3.2. Slope for particles in δ-F-curves decrease with loading rate differently to tips

Finally, the d-F-curves were plotted for the particles. Then, again, linear fittings with ranges of 0 to 200 pN, 200 to 400 pN, 400 to 600 pN, and 600 to 800 pN were performed. Figure 4-10 shows such fittings for a curve done with 5 µm/s and a maximum load of 2.5 nN with the fittings as dashed lines. Table 4-5 shows the values for the fittings.

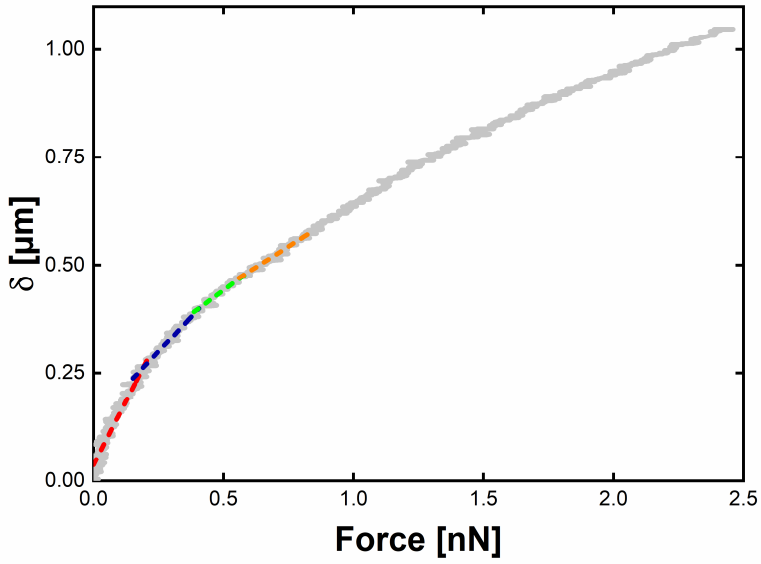

Figure 4-10. Indentation-Force-curve measured for a particle at a loading rate of 5 µm/s and a maximum force of 1 nN. The dashed lines show linear fittings to different curve segments of 0 to 200 pN (red), 200 to 400 pN (blue), 400 to 600 pN (green), and 600 to 800 pN (orange).

Table 4-5. Slopes from indentation-forces curve fittings for the curve shown in Figure 4-10 performed with a spherical particle.

Range (pN)	0 – 200	200 – 400	400 – 600	600 – 800
Slope	1171.0 ± 2.1	640.5 ± 14.0	434.6 ± 12.9	385.0 ± 10.6
Residual Sum of Squares	1.225E-13	1.417E-14	4.371E-15	4.301E-15
R-Squared	0.923	0.93781	0.92775	0.93516
Adj. R-Squared	0.92314	0.93736	0.92694	0.93445

Then, Figure 4-11 shows the derived values from such fittings. The measured slope again decreases both with the loading rate and with the force range. While the slope decreases by a factor of approximately 4 for the tips regarding a force range from 0 to 200 and from 600 to 800, for the same ranges for the particles it decreases approximately by the factor of 3. Table 4-6 then shows the mean values derived for the fittings.

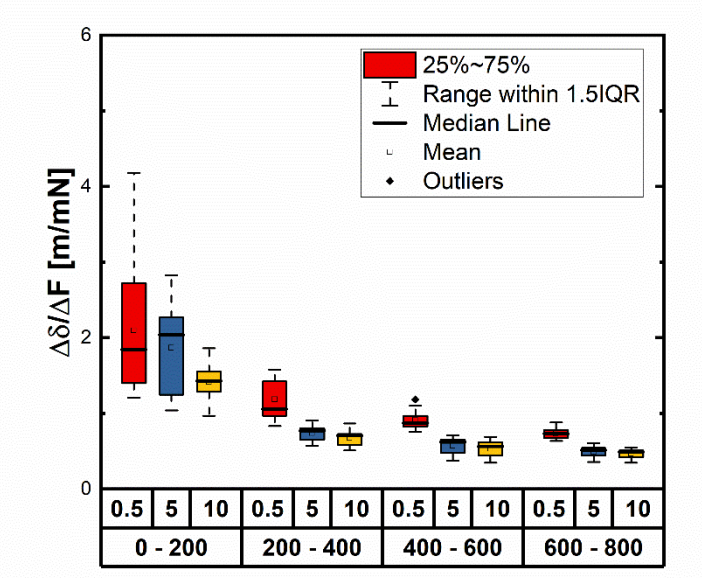

Figure 4-11. Fitted slopes for indentation-force curves in m/mN. In red, the values for loading rates of 0.5 µm/s are shown, in blue for 5 µm/s, and in yellow the ones for 10 µm/s. The measurements were performed with a particle.

Table 4-6. Slopes from various region fittings of δ-F curves performed with a particle at different loading rates in m/mN.

	0.5 µm/s	5 µm/s	10 µm/s
0 – 200 pN	2.10 ± 0.18	1.87 ± 0.10	1.41 ± 0.04
200 – 400 pN	1.18 ± 0.06	0.74 ± 0.02	0.67 ± 0.02
400 – 600 pN	0.92 ± 0.03	0.56 ± 0.02	0.53 ± 0.02
600 – 800 pN	0.74 ± 0.01	0.49 ± 0.01	0.47 ± 0.01

4.4. Young's Modulus determination from F-δ^2 for tip measurements

In a next step, F-δ^2 were plotted for measurements done with tips and F-$\delta^{3/2}$-curves for particles. Then, according to Hertzian theory, linear fittings were performed over the whole indentation range. Since the range is bigger than 10% of the sample (cells are approximately 5.5 µm high), substrate effects will be felt. Figure 4-12 shows such a plot for a measurement made with a tip at 5 µm/s and 1 nN with the fitting. Figure 4-12 (right) shows all fittings for the same settings. The fitting values are shown in Table 4-7. Note that the indentation range shown in the graph corresponds to an indentation of approximately 1.5 µm, which is nearly 30% of the cell height. Surprisingly, the fitting seems to work very well. The fitting shown in

Table 4-7 and Figure 4-12 (left) corresponds to a Young's Modulus of 1.00 kPa. These fittings were then performed for all the curves prepared during this work (Figure 4-13).

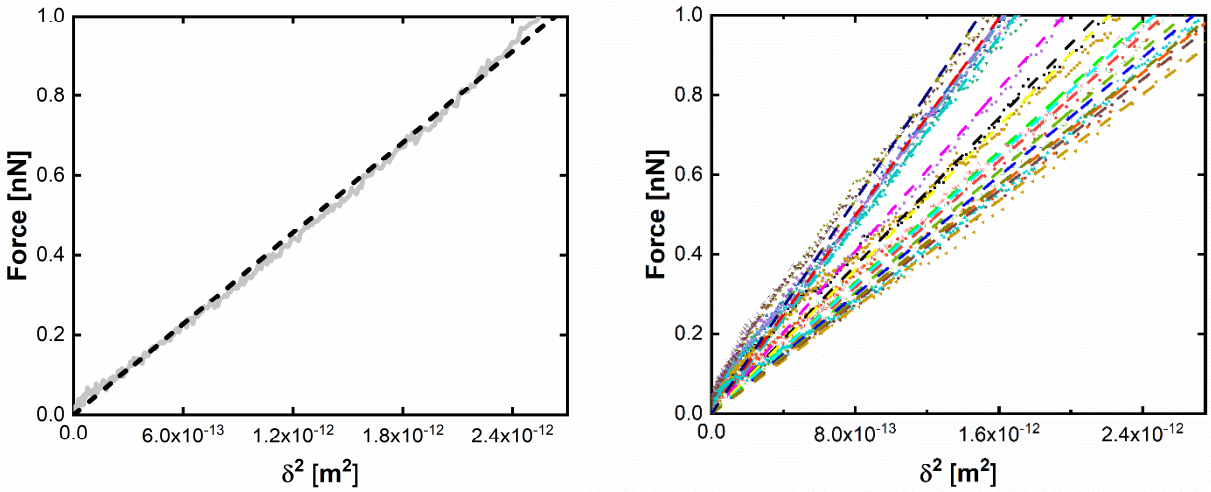

Figure 4-12. Force-δ^2 curves for a single curve (left) and all curves (right) performed at a loading rate of 5 µm/s, 1 nN and with pyramidal tips. The dashed lines correspond to linear fitting where from the slope the Young's Modulus of the sample can be calculated.

Table 4-7. Slope derived from the fitting shown in Figure 4-12 (left) with the statistical values of the fitting.

Slope	**379.9 ± 0.8**
R-squared	0.99876
Adj. R-squared	0.99875

Table 4-8 shows the calculated Young's Modulus values (in kPa ± SEM) for curve fits over the whole measurement range. The difference between the values for the forces can be explained by the increased indentation for higher forces, leading to a deviation from Hertzian theory.

Table 4-8. Determined Young's Modulus values for measurements performed with a pyramidal tip.

	1 nN	**2.5 nN**
0.5 µm/s	0.47 ± 0.02	0.65 ± 0.02
5 µm/s	1.28 ± 0.07	1.37 ± 0.06
10 µm/s	2.33 ± 0.17	2.31 ± 0.12

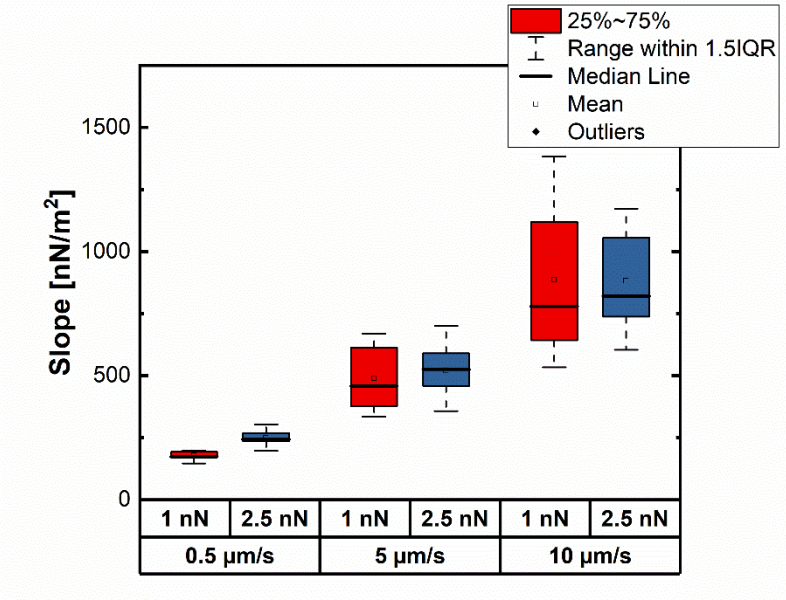

Figure 4-13. Slopes derived from linear fitting of F-δ^2 curves using a tip. In red the values for 1 nN are shown while in blue the values for 2.5 nN are shown.

4.4.1. Young's Modulus depends on indentation depth

The Young's Modulus is supposed to be a material constant. Nevertheless, literature shows that for cell mechanical measurements using AFM, this value seems to depend not only on the loading rate, but also on the respective indentation depth. Therefore, F-δ^2-curves were fitted over a range of 0 to 1,000 nm in segments of 100 nm. An example of such a fitting is shown in Figure 4-14, for a curve with a tip and a 5 µm/s rate. The respective fitting values are shown in Table 4-9. As can be seen, different slopes are visible.

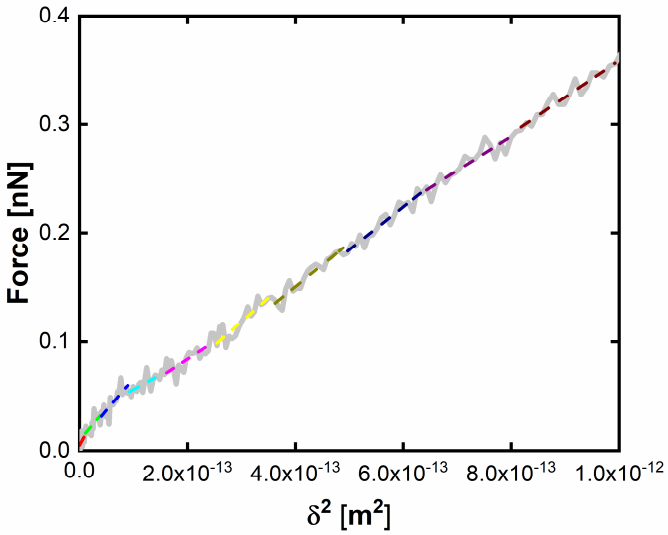

Figure 4-14. Linear fittings over different ranges of the F-δ^2 curve show that the value of the Young's Modulus depends on the indentation depth.

Table 4-9. Slopes derived from fittings over intervals of 100 nm as shown in Figure 4-14.

Depth	Slope	R2
0 – 100	877	0.19
100 – 200	574	0.46
200 – 300	586	0.65
300 – 400	268	0.53
400 - 500	325	0.60
500 – 600	439	0.80
600 – 700	400	0.90
700 – 800	393	0.90
800 – 900	317	0.85
900 – 1,000	340	0.92

This shows that the curve shape appears to be non-linear in the beginning of the indentation. Also, due to the few data-points fitted, the goodness of the fitting is quite decreased. Again, such fittings were performed. This time, only for measurements performed with 5 µm/s and a maximum force of 1 nN. Figure 4-15 shows the result

of this analysis. Apparently, the Young's Modulus is overestimated considering only the first few hundred nm of the measurements.

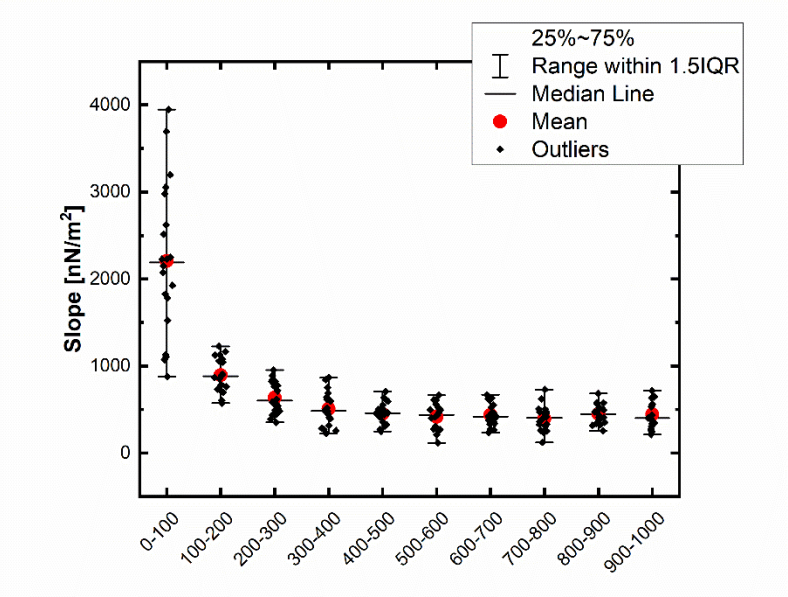

Figure 4-15. Slope values for the different stiffness regions determined for measurements using a pyramidal tip.

4.5. Young's Modulus determination from F-$\delta^{3/2}$ curves for particle measurements

Like the evaluation done for the tip measurements, measurements with the particles were evaluated to determine the Young's Modulus. For this, F-$\delta^{3/2}$ curves

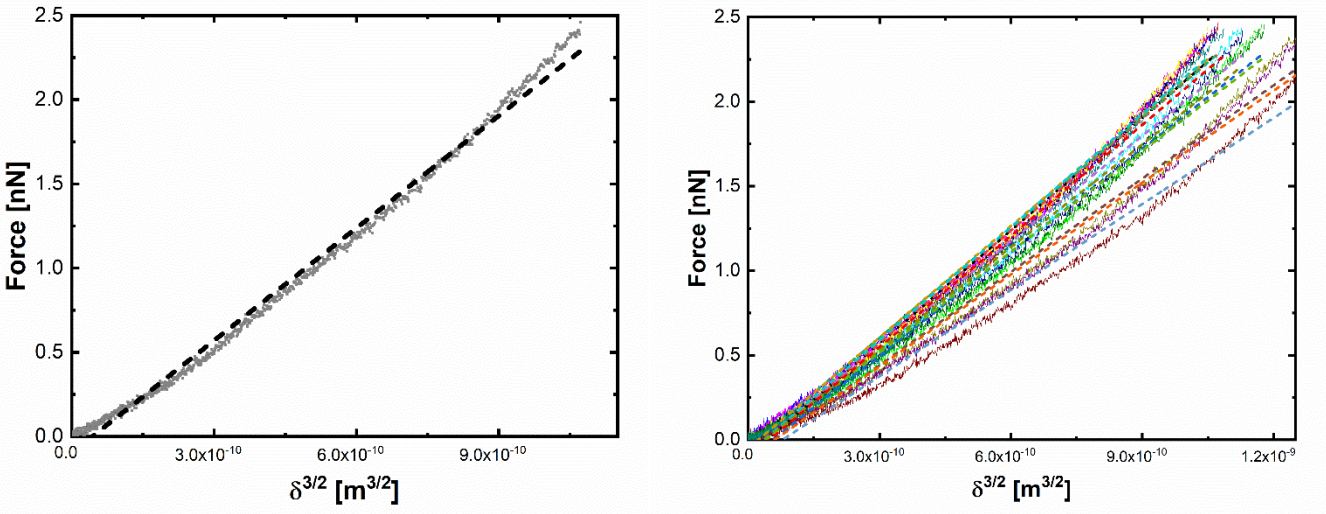

Figure 4-16. Force-$\delta^{3/2}$ curves for a single curve (left) and all curves (right) performed at a loading rate of 5 µm/s, 2.5 nN and with a particle. The dashed lines correspond to linear fitting where from the slope the Young's Modulus of the sample can be calculated.

were plotted. Then, linear fittings of this curves were performed. Such fittings should

in theory correspond to Hertzian elastic mechanics. Figure 4-16 shows such a fitting for a measurement with a 10 µm diameter silica particle done at 5 µm/s and a maximum force of 2.5 nN. In Figure 4-16 (right) this fitting can be seen for all the curves performed as such settings. Comparing such fittings to the ones done with the tip, it looks like the fitting does not work that well. The values of the fitting are shown in Table 4-10. The calculated Young's Modulus for the slope shown in Table 4-10 is 0.56 kPa.

Table 4-10. Slope derived from the fitting shown in Figure 4-16 (left) with the statistical values of the fitting.

Slope	**2.22 ± 0.01**
R-squared	0.99356
Adj. R-squared	0.99355

Table 4-11 shows the calculated Young's Modulus values for the measurements, considering the fitted slopes over the whole data range as well as the particle radius. The Young's Modulus increases non-linearly with the loading rate. Interestingly, it increases with the maximum force. Here the indentation range should be considered in detail. The result of the slope fittings can be seen in Figure 4-17.

Table 4-11. Determined Young's Modulus values for measurements performed with a particle.

	1 nN	**2.5 nN**
0.5 µm/s	0.13 ± 0.01	0.32 ± 0.01
5 µm/s	0.23 ± 0.01	0.52 ± 0.01
10 µm/s	0.34 ± 0.01	0.61 ± 0.01

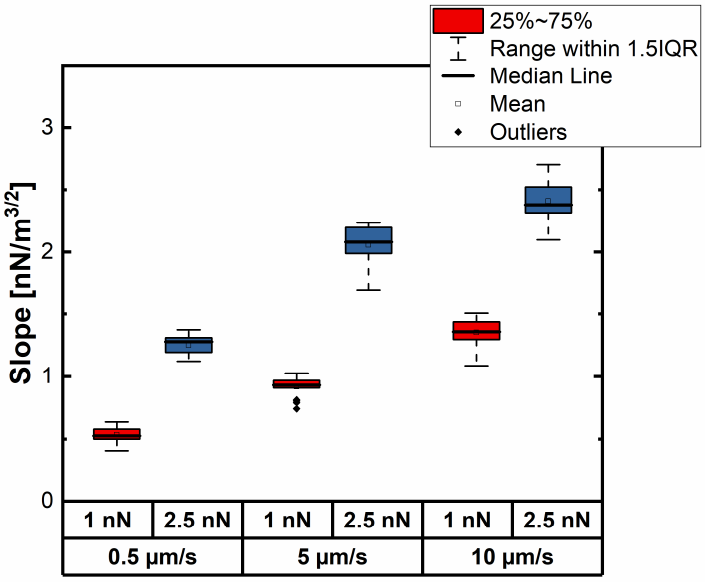

Figure 4-17. Slopes derived from linear fitting of F-$\delta^{3/2}$ curves using a particle. In red the values for 1 nN are shown while in blue the values for 2.5 nN are shown.

4.5.1. Indentation depth plays a bigger role for Young's modulus when using particles

Next, the dependence of the indentation depth of the slope/Young's modulus when using particles was evaluated. Here again, fittings in the interval of 100 nm were performed over indentation ranges of 0 to 1 µm (when possible). Such a fitting is show in Figure 4-18, measured at 5 µm/s and 2.5 nN maximum force. The corresponding fitted functions are seen in Table 4-12.

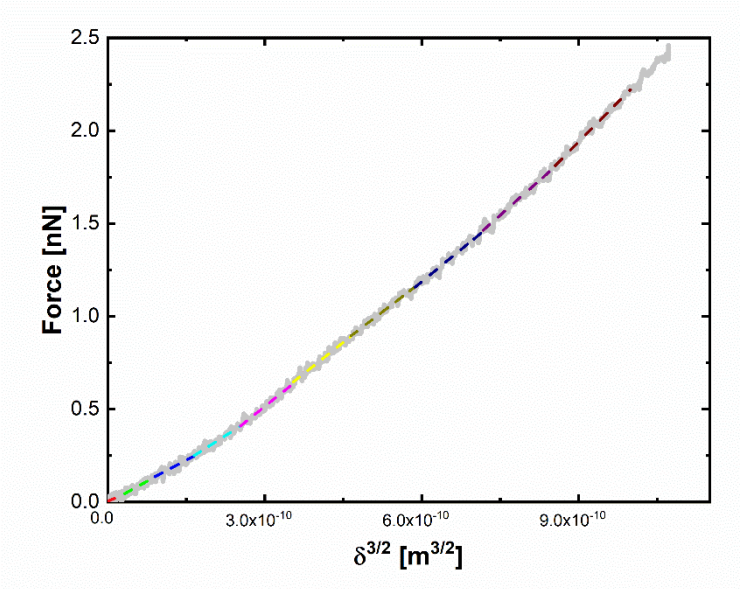

Figure 4-18. Linear fittings over different ranges of the F-$\delta^{3/2}$ curve show that the Young's Modulus depends on the indentation depth for particle measurements.

Table 4-12. Slopes derived from fittings over intervals of 100 nm as shown in Figure 4-18.

Depth	Slope	R2
0 – 100	1.15	0.36
100 – 200	1.55	0.80
200 – 300	1.49	0.81
300 – 400	1.81	0.91
400 - 500	2.27	0.95
500 – 600	2.22	0.95
600 – 700	2.16	0.96
700 – 800	2.31	0.96
800 – 900	2.49	0.96
900 – 1,000	2.85	0.98

Interestingly, the slope seems to gradually increase with the indentation. This contrasts with the results shown before for the measurements done with a tip. Probably, at such indentations, the substrate is felt more and more. The same

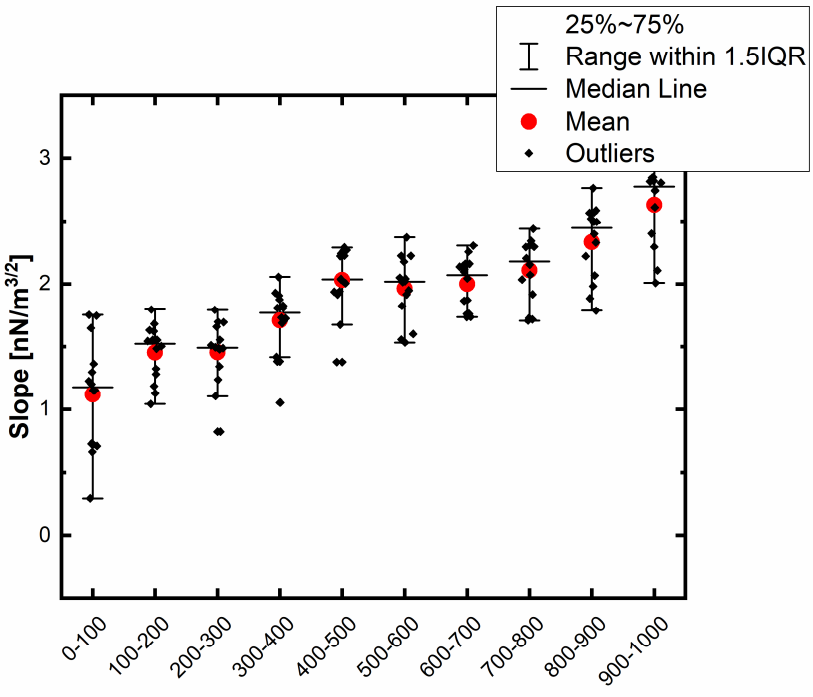

Figure 4-19. Slope values for the different stiffness regions determined for measurements using a pyramidal tip.

behavior is visible when evaluating all the curves, as can be seen in Figure 4-19.

5. Conclusion

In this thesis, the influence of different measurement settings on the mechanical properties of cells measured with Atomic Force Microscopy was tested. This was done by variation of the loading rate and the maximum force. In addition, either a pyramidal tip or a 10 µm diameter silica particle was used. From such measurements, then as a first step, the curve shape and maximum indentation was evaluated. In succession, slopes of both Force-distance and indentation-distance curves were fitted to check if there are differences. Finally, by plotting F-δ^2 and F-$\delta^{3/2}$ curves, the Young's Modulus of the cells was determined.

Following influences of the measurement settings on the derived parameters were determined:

- Independently of the used indenter geometry, the measured stiffness properties of the cells increased with the loading rate in a non-linear fashion,
- When measuring with a particle cells appear softer then when measuring with a tip,
- Due to the pressure distribution it takes more force when using particles to reach the same depth of indentation when using tips,
- Young's Modulus is both loading rate and indentation dependent,
    - For tips, at very low indentations, a higher Young's Modulus is measured. This is probably due to the effect that at low indentations the tip shape appears more spherical (considering indentations of a few hundred nanometers and a tip radius of 20 nm),
    - For particles, the measured Young's Modulus increases non-linearly with the indentation depth. This effect is probably attributed effects from the substrate and should be corrected for using the appropriate contact models.

As an outlook one should consider performing a similar analysis with a comparison of the approach and the retracting curve, this enabling one to look at viscoelastic properties when considering such effects as hysteresis. Further, performance of F-t

curve with pause segments (holding at constant force or at constant indentation) could be used to derive viscoelastic cell properties.

6. Bibliography

1. Fletcher, D. A. & Mullins, R. D. Cell mechanics and the cytoskeleton. *Nature* **463**, 485–92 (2010).

2. Wang, N. *et al.* Mechanical behavior in living cells consistent with the tensegrity model. *Proc. Natl. Acad. Sci.* **98**, 7765–7770 (2001).

3. Ingber, D. E., Wang, N. & Stamenović, D. Tensegrity, cellular biophysics, and the mechanics of living systems. *Reports Prog. Phys.* **77**, 046603 (2014).

4. Ahmed, W. W., Fodor, É. & Betz, T. Active cell mechanics: Measurement and theory. *Biochim. Biophys. Acta - Mol. Cell Res.* **1853**, 3083–3094 (2015).

5. Gkretsi, V., Stylianou, A., Louca, M. & Stylianopoulos, T. Identification of Ras suppressor-1 (RSU-1) as a potential breast cancer metastasis biomarker using a three-dimensional in vitro approach. **8**, 27364–27379 (2017).

6. Yim, E. K. F., Darling, E. M., Kulangara, K., Guilak, F. & Leong, K. W. Nanotopography-induced changes in focal adhesions, cytoskeletal organization, and mechanical properties of human mesenchymal stem cells. *Biomaterials* **31**, 1299–1306 (2010).

7. Kalli, M. & Stylianopoulos, T. Defining the Role of Solid Stress and Matrix Stiffness in Cancer Cell Proliferation and Metastasis. **8**, (2018).

8. Ondeck, M. G. *et al.* Dynamically stiffened matrix promotes malignant transformation of mammary epithelial cells via collective mechanical signaling. *Proc. Natl. Acad. Sci.* **116**, 3502 LP – 3507 (2019).

9. Krieg, M. *et al.* Atomic force microscopy-based mechanobiology. *Nat. Rev. Phys.* **1**, 41–57 (2019).

10. Lim, C. T., Zhou, E. H. & Quek, S. T. Mechanical models for living cells - A review. *J. Biomech.* **39**, 195–216 (2006).

11. Missirlis, Y. F. Mechanoepigenetics. *Front. Cell Dev. Biol.* **4**, 10–13 (2016).

12. Suresh, S. Biomechanics and biophysics of cancer cells. *Acta Biomater.* **3**, 413–438 (2007).

13. Gavara, N. A beginner's guide to atomic force microscopy probing for cell mechanics. *Microsc. Res. Tech.* **80**, 75–84 (2017).

14. Gavara, N. A beginner's guide to atomic force microscopy probing for cell mechanics. *Microscopy Research and Technique* vol. 80 75–84 (2017).

15. Carl, P. & Schillers, H. Elasticity measurement of living cells with an atomic force microscope: data acquisition and processing. *Pflugers Arch.* **457**, 551–559 (2008).

16. Lekka, M. Discrimination Between Normal and Cancerous Cells Using AFM. *Bionanoscience* **6**, 65–80 (2016).

17. Stamenovic, D. Microtubules may harden or soften cells, depending of the extent of cell distension. *J. Biomech.* **38**, 1728–1732 (2005).

18. Wu, H. W., Kuhn, T. & Moy, V. T. Mechanical properties of L929 cells measured by atomic force microscopy: effects of anticytoskeletal drugs and membrane crosslinking. *Scanning* **20**, 389–397 (1998).

19. Rotsch, C. & Radmacher, M. Drug-induced changes of cytoskeletal structure and mechanics in fibroblasts: an atomic force microscopy study. *Biophys. J.* **78**, 520–535 (2000).

20. Rotsch, C., Braet, F., Wisse, E. & Radmacher, M. AFM imaging and elasticity measurements on living rat liver macrophages. *Cell Biol. Int.* **21**, 685–696 (1997).

21. Benitez, R. & Toca-herrera, J. L. Looking at cell mechanics with atomic force microscopy: Experiment and theory. *Microsc. Res. Tech.* **77**, 947–958 (2014).

22. Efremov, Y. M., Bagrov, D. V., Kirpichnikov, M. P. & Shaitan, K. V. Application of the Johnson-Kendall-Roberts model in AFM-based mechanical measurements on cells and gel. *Colloids Surfaces B Biointerfaces* **134**, 131–139 (2015).

23. Darling, E. M., Zauscher, S. & Guilak, F. Viscoelastic properties of zonal articular chondrocytes measured by atomic force microscopy. *Osteoarthr. Cartil.* **14**, 571–579 (2006).

24. Alcaraz, J. *et al.* Microrheology of human lung epithelial cells measured by atomic force microscopy. *Biophys. J.* **84**, 2071–2079 (2003).

25. López-Guerra, E. A. & Solares, S. D. Modeling viscoelasticity through spring-dashpot models in intermittent-contact atomic force microscopy. *Beilstein J. Nanotechnol.* **5**, 2149–2163 (2014).

26. Hiratsuka, S. *et al.* Power-law stress and creep relaxations of single cells measured by colloidal probe atomic force microscopy. *Jpn. J. Appl. Phys.* **48**, (2009).

27. Moreno-Flores, S., Benitez, R., Vivanco, M. dM & Toca-Herrera, J. L. Stress relaxation and creep on living cells with the atomic force microscope: a means to calculate elastic moduli and viscosities of cell components. *Nanotechnology* **21**, 445101 (2010).

28. Ingber, D. E. Cellular tensegrity: defining new rules of biological design that govern the cytoskeleton. *J. Cell Sci.* **104 (Pt 3**, 613–627 (1993).

29. Guz, N., Dokukin, M., Kalaparthi, V. & Sokolov, I. If Cell Mechanics Can Be Described by Elastic Modulus: Study of Different Models and Probes Used in Indentation Experiments. *Biophys. J.* **107**, 564–575 (2014).

30. Wu, P.-H. *et al.* A comparison of methods to assess cell mechanical properties. *Nat. Methods* **15**, 491–498 (2018).

31. Schmid-Schönbein, G. W., Sung, K. L., Tözeren, H., Skalak, R. & Chien, S. Passive mechanical properties of human leukocytes. *Biophys. J.* **36**, 243–256 (1981).

32. Zhang, G., Long, M., Wu, Z.-Z. & Yu, W.-Q. Mechanical properties of hepatocellular carcinoma cells. *World J. Gastroenterol.* **8**, 243–246 (2002).

33. Sato, M., Theret, D. P., Wheeler, L. T., Ohshima, N. & Nerem, R. M. Application of the micropipette technique to the measurement of cultured porcine aortic endothelial cell viscoelastic properties. *J. Biomech. Eng.* **112**, 263–268 (1990).

34. Wullkopf, L. *et al.* Cancer cells' ability to mechanically adjust to extracellular matrix stiffness correlates with their invasive potential. *Mol. Biol. Cell* **29**, 2378–2385 (2018).

35. Neuman, K. C. & Nagy, A. Single-molecule force spectroscopy: optical tweezers, magnetic tweezers and atomic force microscopy. *Nat. Methods* **5**, 491 (2008).

36. Butt, H. J., Cappella, B. & Kappl, M. Force measurements with the atomic force

microscope: Technique, interpretation and applications. *Surf. Sci. Rep.* **59**, 1–152 (2005).

37. Butt, H.-J. & Jaschke, M. Calculation of thermal noise in atomic force microscopy. *Nanotechnology* **6**, 1–7 (1995).

38. Weber, A., Iturri, J., Benitez, R. & Toca-Herrera, J. L. Measuring biomaterials mechanics with atomic force microscopy. 1. Influence of the loading rate and applied force (pyramidal tips). *Microsc. Res. Tech.* **82**, 1392–1400 (2019).

39. Butt, H.-J., Cappella, B. & Kappl, M. Force measurements with the atomic force microscope: Technique, interpretation and applications. *Surf. Sci. Rep.* **59**, 1–152 (2005).

40. Efremov, Y. M., Bagrov, D. V., Kirpichnikov, M. P. & Shaitan, K. V. Application of the Johnson-Kendall-Roberts model in AFM-based mechanical measurements on cells and gel. *Colloids Surfaces B Biointerfaces* **134**, 131–139 (2015).

41. Butt, H.-J. & Jaschke, M. Calculation of thermal noise in atomic force microscopy. *Nanotechnology* **6**, 1–7 (1995).

7. List of Figures

Figure 3-5. Correction steps of Force-distance-curves. (a) Raw Force-distance-curve, in red the approach and in blue the retract can be seen. (b) Baseline correction of the curve and tilting of the baseline. (c) Definition of contact point. (d) Correction for the bending of the cantilever.

Figure 3-6. (a) Single F-d-curve after full correction. (b) Multiple F-d-curves for the same settings showing that the measurements look similar and data can be pooled.

Figure 3-7. (a) Force-δ^2-curve for a single curve performed with a pyramidal tip cantilever and (b) all the curves for the same measurement settings. (c) Force- $\delta^{3/2}$-curve for a single curve performed with a spherical particle and (d) all the curves performed for such measurement settings.

Figure 4-1. Force distance curves of measurements performed using a pyramidal tip as an indenter. Top row shows those done at 0.5 µm/s (1 nN left and 2.5 nN right), middle show shows those done with 5 µm/s (1 nN left and 2.5 nN right) and the bottom row shows those performed using a rate of 10 µm/s.

Figure 4-2. Force distance curves of measurements performed using a particle as an indenter. Top row shows those done at 0.5 µm/s (1 nN left and 2.5 nN right), middle show shows those done with 5 µm/s (1 nN left and 2.5 nN right) and the bottom row shows those performed using a rate of 10 µm/s.

Figure 4-3. Maximum indentations at the given measurement settings for particle measurements (left) and pyramidal tip measurements (right). In red, measurements using 1 nN maximum force are shown while in red it is the ones with 2.5 nN. All the used loading rates are shown.

Figure 4-4. Force distance curve of a measurement performed with a particle and a loading rate of 5 µm/s and a maximum force of 1 nN. The grey line indicates the measurement while the dashed lines show a fitting over a range of 0 to 200 nm (red), 200 to 400 nm (blue) and 400 to 800 nm (green). The fitting performed was a linear fitting.

Figure 4-5. Calculated measured stiffness values from Force-distance curve fittings over ranges of 0 to 200, 200 to 400 and 400 to 800 nm for the different loading rates. Note that the measurements for 1 and 2.5 nN were pooled.

Figure 4-15. Slope values for the different stiffness regions determined for measurements using a pyramidal tip.

Figure 4-16. Force-$\delta^{3/2}$ curves for a single curve (left) and all curves (right) performed at a loading rate of 5 µm/s, 2.5 nN and with a particle. The dashed lines correspond to linear fitting where from the slope the Young's Modulus of the sample can be calculated.

Figure 4-17. Slopes derived from linear fitting of F-$\delta^{3/2}$ curves measured using a colloidal particle. In red the values for 1 nN are shown, while the values for 2.5 nN are shown in blue.

Figure 4-18. Linear fittings over different ranges of the F-$\delta^{3/2}$ curve show that the Young's Modulus depends on the indentation depth for particle measurements.

8. List of Tables

9. Acknowledgements

First of all, I would like to thank to Professor José Luis Toca-Herrera for the great opportunity to perform my Master thesis under his supervision. I am thankful to the fate that he brought me and my family with him.

My sincere thanks also go to DI Andreas Weber who supported me right from the start of my thesis. I am especially grateful for his great presentations, help in reviewing drafts of the thesis and comprehensive assistance.

I want to thank Professor Gerhard Schütz for help in the study of cell biology and for his fascinating lectures.

I wish to say a special thanks to Dean of Biomedical Engineering Professor Eugenijus Kaniusas and the International office of TU Wien for help in administrative issues.

This long journey couldn't have happened without my family and their support.

Furthermore, for financial support I would like to thank Russian government funding program “Global Education Program (GEP)”.